FEASIBILITY DEMONSTRATION OF LOW FREQUENCY ACOUSTO-OPTICAL IMAGING FOR SONAR APPLICATIONS

R. A. Smith, et al

TRW Systems Group

Prepared for:

Advanced Research Projects Agency

12 July 1973

Unclassified
Security Classification

AD-768 398

DOCUMENT CONTROL DATA - R & D

(Security classification of title, body of abstract and indexing annotation must be entered when the overall report is classified)

1. ORIGINATING ACTIVITY *(Corporate author)*
TRW Systems Group
One Space Park
Redondo Beach, California 90278

2a. REPORT SECURITY CLASSIFICATION
Unclassified

2b. GROUP

3. REPORT TITLE
Feasibility Demonstration of Low Frequency Acousto-Optical Imaging for Sonar Applications

4. DESCRIPTIVE NOTES *(Type of report and inclusive dates)*
Interim Report, Phase I, January 1972 to June 1973

5. AUTHOR(S) *(First name, middle initial, last name)*
R. A. Smith, J. H. Cole, R. L. Johnson, P. G. Bhuta

6. REPORT DATE	7a. TOTAL NO. OF PAGES	7b. NO. OF REFS
12 July 1973	~~107~~ 109	16

8a. CONTRACT OR GRANT NO	9a. ORIGINATOR'S REPORT NUMBER(S)
N00014-72-C-0182	
b. PROJECT NO. 463	AT-SVD-TR-73-10
c. Purchase Request NR 240-030	9b. OTHER REPORT NO(S) *(Any other numbers that may be assigned this report)*
d. Dated 11-09-71	

10. DISTRIBUTION STATEMENT
For Public Release.

11. SUPPLEMENTARY NOTES	12. SPONSORING MILITARY ACTIVITY
Robert Obrochta ONR Scientific Officer (201) 692-4413	Defense Advanced Research Projects Agency

13. ABSTRACT

Analysis and experiments were performed to prove the feasibility of an underwater imaging system based on acousto-optical imaging for sonar applications at frequencies from 25 to a few hundred KHz. Experimental results confirming sensitivity and resolution are presented together with images of insonified objects at a distance of 15 feet (the maximum allowed by the size of the test facility). A novel heterodyning technique was devised to perform low frequency imaging. Based upon the laboratory experiments, range and resolution achievable with the acousto-optical imaging sonar are estimated. Construction of a high resolution acousto-optical imaging sonar is entirely feasible.

DD FORM 1 NOV 65 1473

Unclassified
Security Classification

14 KEY WORDS	LINK A		LINK B		LINK C	
	ROLE	WT	ROLE	WT	ROLE	WT
Sonar						
Imaging						
Ocean Surveillance						
Bragg Imaging						
Underwater inspection system						
Raman-Nath Imaging						

TRW
SYSTEMS GROUP

FEASIBILITY DEMONSTRATION OF LOW FREQUENCY ACOUSTO-OPTICAL IMAGING FOR SONAR APPLICATIONS

INTERIM REPORT FOR PHASE I

(January 1972 - June 1973)

12 July 1973

AT-SVD-TR-73-10

by

R. A. Smith, J. H. Cole
R. L. Johnson and P. G. Bhuta
Advanced Technology Staff
Space Vehicles Division

Sponsored by

Defense Advanced Research Projects Agency
Arlington, Virginia 22209

ARPA Order No. 1959
Program Code No. 3N10

Prepared for

Office of Naval Research
Arlington, Virginia

Contract No. N00014-72-C-0182
NR 230-030

TRW SYSTEMS GROUP
One Space Park
Redondo Beach, California 90278

For Public Release

TRW

FOREWORD

This report was prepared by the Advanced Technology Staff, Space Vehicles Division, TRW Systems Group, Redondo Beach, California, under contract N00014-72-C-0182 with the Office of Naval Research, Arlington, Virginia. The project was sponsored by the Defense Advanced Research Projects Agency under ARPA Order number 1951. The authors wish to thank Mr. Robert Obrochta, Code 463, Surface and Amphibious Programs, Naval Applications Analysis Division, ONR, for the valuable technical discussions and the guidance provided during the course of this investigation. The authors also wish to acknowledge the assistance provided by Mr. Cliff Murrow in performing the laboratory experiments. Technical discussions with Drs. Ernest Blase and Jeff Fenton of Naval Intelligence Support Center provided valuable insight into potential applications of this new technology. Informal technical interchange with Dr. Tom Muir, Applied Research Laboratory, University of Texas, provided the authors with background information concerning the current state of the art of conventional sonars. The authors wish to thank Dr. Tom Muir for his assistance in this area.

TRW SYSTEMS GROUP

TABLE OF CONTENTS

TRW SYSTEMS GROUP

LIST OF FIGURES

TRW SYSTEMS GROUP

LIST OF FIGURES (Cont.)

LIST OF FIGURES (Cont.)

TRW
SYSTEMS GROUP

LIST OF TABLES

TRW
SYSTEMS GROUP

1.0 INTRODUCTION AND SUMMARY

The technical problem addressed under this program is the extension of acousto-optical imaging techniques to the frequency range of interest for DoD underwater applications. Previous investigations of acousto-optical imaging have been carried out with objects insonified by sound at frequencies of 4 MHz or greater[1,2,3,4,5]. Under this contract TRW has formed good optical images of targets insonified with sound at frequencies as low as 280 KHz. In addition, imaging by using light heterodyne pickup was conceived and demonstrated using a single detector scan. This technique, when developed, should permit the formation of acousto-optical images at frequencies as low as 25 KHz. This constitutes a major breakthrough in the technology of forming optical images from acoustic wave fronts.

The methodology followed under this contract was primarily experimental, analyses being performed as necessary to guide experiment and verify results. A Bragg cell (region of interaction of light and sound waves) was installed at one end of TRW Systems' large wave tank. Targets were mounted at the opposite end of the tank and insonified by transducers located near the aperture. Sound reflected by targets interacted with the laser light in the Bragg cell resulting in optical sidebands containing an image of the insonified target. The sidebands were processed to display the image on TV or on photographic film. Laboratory results are summarized in Section 3.0.

The DoD implications of this work are as follows. The High Resolution Sonar Study Panel of the Mine Advisory Committee[6] considered the value of two-dimensional imaging for Naval underwater applications and concluded that the capability would provide tactical advantage for several applications if it could be performed at ranges of from 100 to 500 yards. The principal application at these ranges is mine hunting and swimmer detection. In addition there are short range applications (object identification, ship hull inspection) which can be performed at higher frequencies. As a result

of this project, the feasibility of forming two dimensional images acousto-optically on long ranges has been demonstrated. This is demonstrated by the experimental results in Section 3.0.

Theoretically the field of view of a light wedge operating as an acousto-optic receiver is equal to the wedge angle. Work carried out during this phase of the project tend to verify this. The wedge angle which can be obtained in practice is limited by practical consideration of lens size. As a result with a single wedge system the field of view is limited to about 30°. System designs which would extend the instantaneous field of view to 90° or greater have been conceived by TRW but were not investigated under this phase of the contract.

2.0 BASIC PRINCIPLES OF OPERATION

Essential elements characterizing the imaging system investigated here are shown in Figure 1. The object to be viewed is assumed to be illuminated only by sound which is reflected into a column of laser light having the shape of a wedge. This wedge of light is formed by the cylindrical lens (at left) intercepting collimated light from an Argon-ion laser. The shape of the object in the sound field is replicated in light diffracted out of this wedge of light. The cylindrical lens on the right is required to form an image which is properly proportioned. Figure 2 shows some images formed by this system early in the project. The object illuminated only by sound (Figure 2a) was placed quite near the light-sound interaction region. Most of the effort reported here was given to the formation of images of objects located at a distance of 15 ft from the light-sound interaction region.

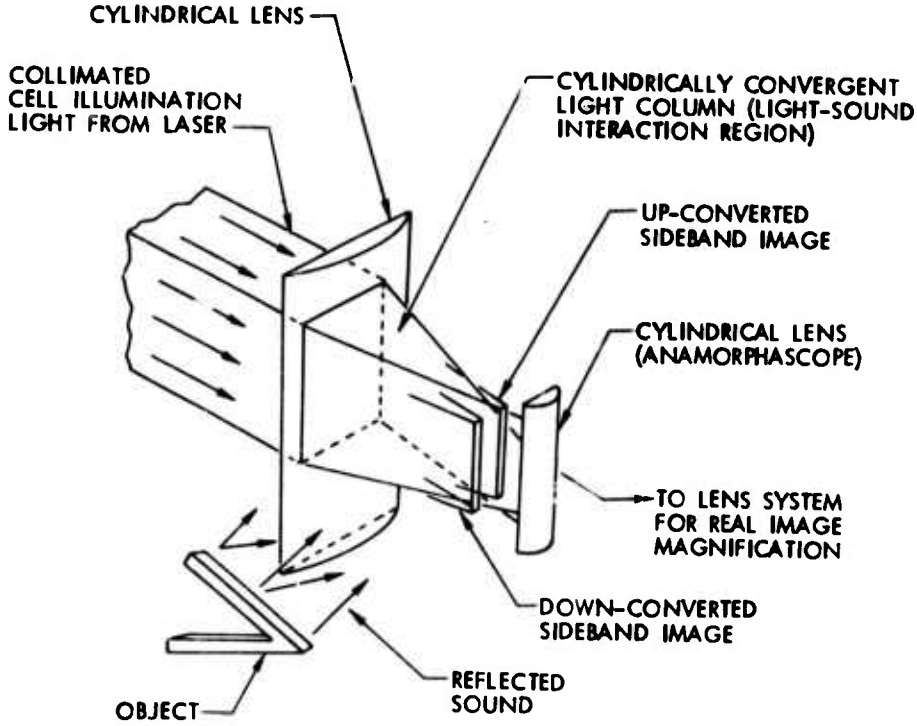

Figure 1: Bragg imaging elements

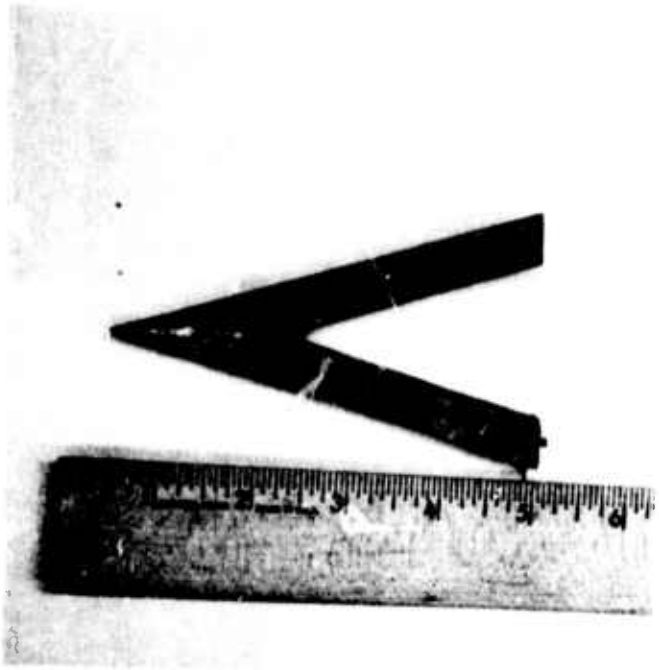

Figure 2a: Object used in the TRW Bragg imaging system to form the images below.

410 KHz 695 KHz 975 KHz

Figure 2b: Images formed by sound reflected from the object above using sound at the indicated frequency.

2.1 Working Principles of Low Frequency Acousto-Optical Imaging

There is a long wavelength limit below which Bragg diffraction (as commonly defined) cannot occur. This long wavelength limit follows from a previously published definition of Bragg diffraction due to ultrasound[7]. It reduces to the requirement that a light ray in the interaction region must cross at least one wavelength of sound as illustrated in Figure 3. Both the incident and diffracted light rays are oriented to satisfy the angular relation specified by the Bragg condition (as shown in Figure 3).

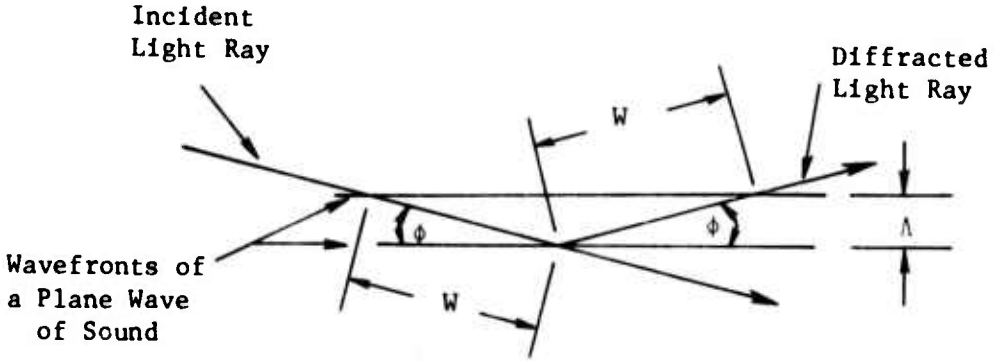

where $\phi = \sin^{-1} \frac{\lambda}{2\Lambda}$

λ = light wavelength

Λ = sound wavelength

Figure 3: Bragg diffraction (due to sound) from only two wave fronts.

Inspection of Figure 3 reveals

$$W \sin \phi = \frac{W\lambda}{2\Lambda} = \Lambda \tag{1}$$

It is evident from Figure 1 that the width of interaction must be at least as large as W. A requirement for Bragg diffraction is therefore (from Equation 1)

$$\Lambda < \sqrt{W\lambda/2} \tag{2}$$

For example, assuming cell illumination light is at a wavelength of .54 μM in air and an interaction length of 1.2 meters, the longest sound wavelength that can be considered to diffract light in the Bragg manner is .5 millimeter in water. This corresponds to a minimum sound frequency of 3 megahertz in water. It is then surprising that recognizable images have been formed in a Bragg imaging system at a frequency as low as 500 KHz using a "Bragg" cell which is only 1.2 meters in width. Figure 4 shows an image which was formed from 500 KHz sound reflected at a distance of 15 feet. The object reflecting the sound was a flat cutout having the shape of a submarine with a maximum dimension of 50 cm, as shown in Figure 4. Resolution of the system for an object at the imaging distance (15 feet) was about 9 cm at 500 KHz. The 7.3 cm projection on the object appears with an image dimension determined mostly by resolution alone rather than dimension of the object. That is, reduction of the width of the projection to less than 7.3 cm is expected to produce little change in the image. Only parts of the object as large as several resolution cells show up with image dimensions approximately proportional to object dimensions.

2.1.1 Raman-Nath Imaging

Our interest in this report is limited to low frequencies in a light-sound interaction volume of reasonable dimensions. This places the interaction between light and sound within the Raman-Nath regime. Raman-Nath diffraction is defined by the physical limits which

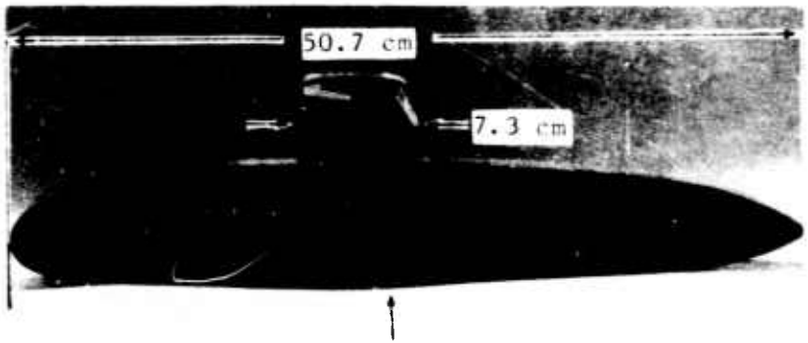

OBJECT USED FOR IMAGES BELOW.

IMAGE OF THE ABOVE OBJECT AT 500 KHz.

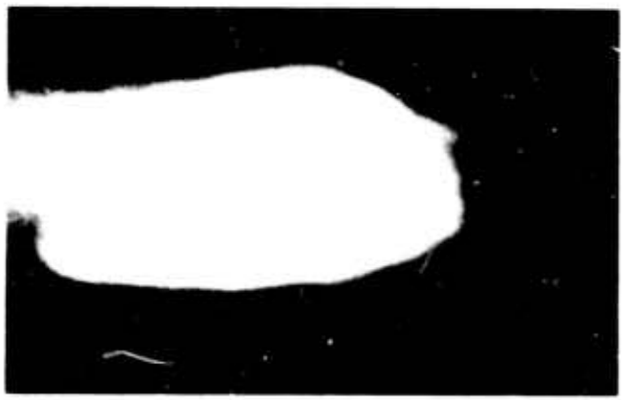

IMAGE OF THE ABOVE OBJECT AT 280 KHz.

Figure 4: Images formed in the TRW Bragg Imaging System with sound reflected from object at a distance of 15 feet.

make the Raman-Nath theory applicable[8]. Raman-Nath theory explains observed diffraction due to sound when the curvature of light rays is negligible. Since we limit our interest to the detection of low amplitude sound, the condition for Raman-Nath diffraction is simply (from Ref. 7)

$$W < \Lambda^2/16\lambda \tag{3}$$

Experiments reported here were done with an Argon-Ion laser operating with λ = .396 μmeter (in water). At a sound wavelength of .3 cm (500 KHz in water) Eq. (3) limits the length of the interaction region for Raman-Nath theory to less than 1.42 meters. Experiments were performed with a shorter interaction length and lower frequencies than 500 KHz. Imaging has been demonstrated which depends upon Raman-Nath diffraction theory.

A ray-tracing analysis of image formation is essentially the same for Raman-Nath and Bragg diffraction. In either regime, the angle through which light is diffracted is the same. The major difference is that Bragg diffraction only occurs when the angle between propagation vectors describing the incident light and the sound field is equal to the Bragg angle, while the Raman-Nath diffraction is maximum with 90 degrees between incident sound and light propagation vectors. This is of little significance as the sound frequency is reduced since the Bragg angle is proportional to sound frequency. A major phenomenological difference is that two first order sidebands, either side of incident light, must appear simultaneously at equal intensities for Raman-Nath diffraction while Bragg diffraction will produce a sideband on only one side of central order light. Under proper conditions all of the incident light can be diffracted into one sideband in Bragg diffraction but not by Raman-Nath diffraction. The intensity of diffracted light in order q under Raman-Nath conditions behaves according to[7]

$$I_q \propto J_q^2\left(\Delta\phi \frac{\sin\left(\pi\left(\frac{W}{\Lambda}\right)\tan\theta\right)}{\pi\frac{W}{\Lambda}\tan\theta}\right) \tag{4}$$

where θ = angle between the incident light propagation vector and plane of the acoustic wave front. ($\theta = 0°$ when the sound wave and light wave propagation vectors are at right angles and in the same plane.)

W = width of the interaction region.

$\Delta\phi$ = peak phase excursion impressed on the light due to passage of an acoustic wave.

J_q = is the ordinary Bessel function of order q.

Equation (4) is based upon a plane wave of sound at a wavelength, Λ and an interaction width, W. The incident light wave is also plane and propagating in a direction nearly perpendicular to the acoustic wave vector. Inspection of the Bessel function argument shows that it has a maximum value at $\theta = 0°$ and falls off rapidly for small values of θ greater than zero. A measure of the width over which the argument takes on a significant value follows from

$$\pi \frac{W}{\Lambda} \tan \theta = \pi$$

Since W/Λ is a large value for all cases of interest here, we see that the intensity of diffracted light is negligible unless $\theta < \Lambda/W$. That is, light and sound propagation vectors must be at right angles in order for diffracted light to be significant. This is the basis for a ray tracing understanding of image formation under Raman-Nath conditions.

2.1.2 Imaging Principles

Objects illuminated with sound produce (by reflection or scatter) a wave pattern completely analogous to the wave pattern reflected from visually viewed objects. Just as objects visually observed may be described by a distribution of plane waves of light, it is also convenient to describe insonified objects by a distribution of plane waves of sound. This viewpoint simplifies the analysis of acousto-optical imaging systems since individual plane waves can be considered separately.

In order to understand acousto-optical imaging it is only necessary to observe the relation between each individual plane wave in the sound field and the resulting plane wave forming the image in the light field.

Formation of an image from a sound field depends on the existence of light over a range of directions so that each plane wave component in the sound field will be replicated. Plane wave components in a sound field which are absent, of course, do not affect the light, and components in the sound field which find no light moving at right angles to the direction of this component would also be absent from diffracted light. An undistorted image is formed only if all components in the sound field defining the insonified image meet with light which satisfies the right angle condition. In order to provide light necessary for satisfying the right angle condition for all components of interest, the acousto-optic cell is illuminated by cylindrically convergent light. There is then a continuum of light rays describing the light field. An alternate scheme uses spherically convergent light to provide a continuum of light rays describing the light field. In either scheme, a range of sound field vectors will encounter light satisfying the right angle condition. The cylindrically convergent light pattern has been found to be much superior at low frequencies and was used to obtain all results presented here.

Any object can be thought of as a collection of points. The imaging of an arbitrary object can be understood by considering the imaging of one point. An object in the form of a single point source can be considered as the superposition of a uniform distribution of plane waves. These plane waves diverge from that point. The wave vectors describing each plane wave then appear as rays. These rays are no different than rays used in geometric optics. Of course, the interpretation differs.

In order to understand the replication of an insonified object in a light field, consider rays in a horizontal plane where that horizontal plane is oriented symmetrically with respect to the ends of the illuminating light field (see Figure 5). Imaging in a direction normal to the

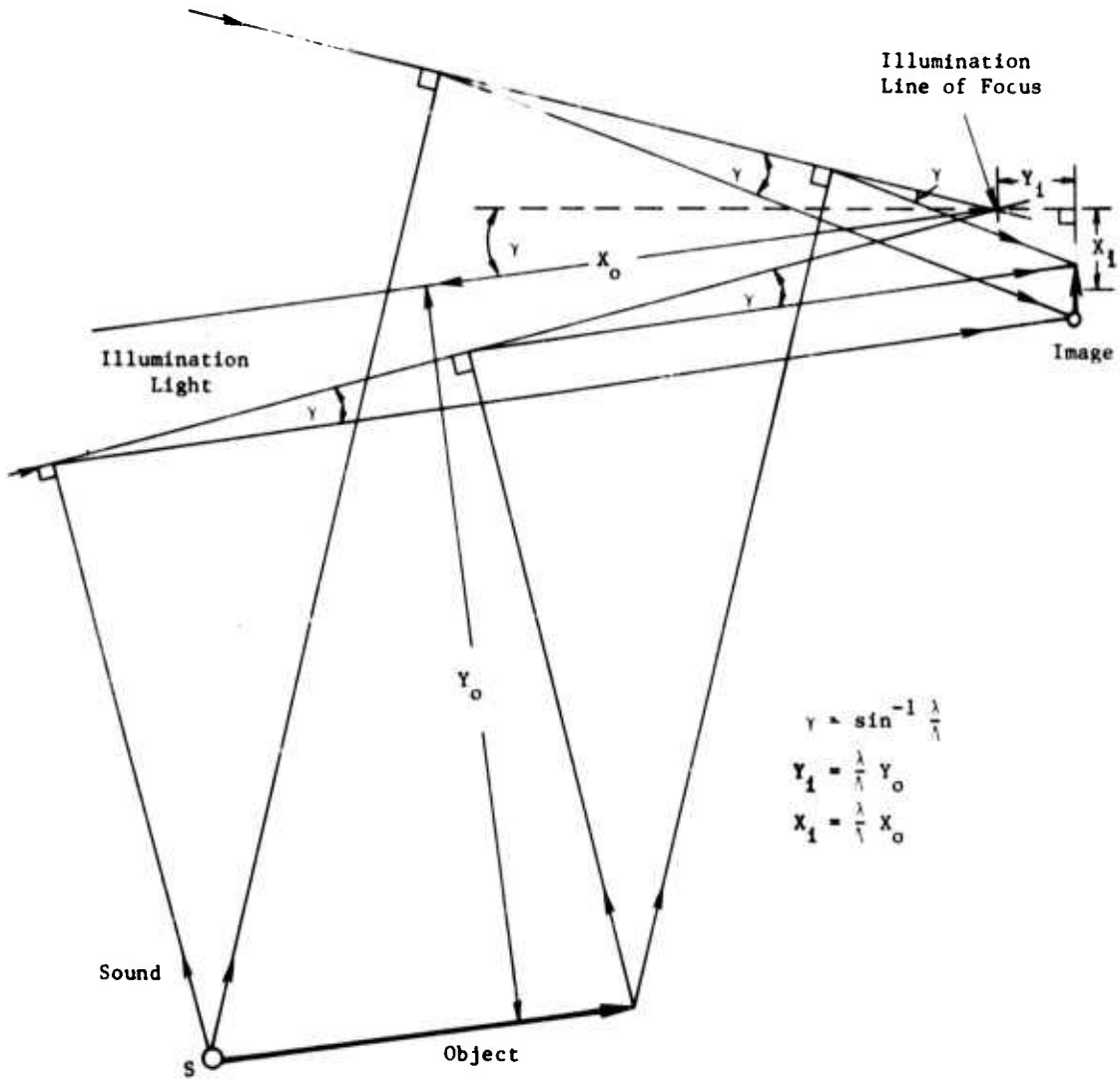

Figure 5: Ray theory of image formation based upon Raman-Nath diffraction.

to the paper in Figure 5 depends upon the imaging of sound (within the light column) in this direction. The imaging property of the light-sound interaction is in the plane of the paper (or other parallel planes). In Figure 5 the inscnified object is an arrow. Sound rays which emanate from a tip of the arrow are shown diverging into the acousto-optic cell. The cell in this figure is defined by the location of the convergent light rays. This figure was constructed by locating mutually perpendicular rays and subsequently constructing rays at an angle $\gamma = \sin^{-1}(\lambda/\Lambda)$ with respect to an incident light ray. The angle between diffracted light rays and sound rays is precisely the complement of γ. Along any given sound ray only one light ray is encountered which satisfies this condition. Only this component produces a diffracted light ray which subsequently forms the image. Note that sound rays emanating from a point produce diffracted light rays that converge to a point. All convergent rays related to a specific point on the object will meet a specific point on the image. In this way, point-for-point an entire object will be replicated in the image. Mathematical analysis of the geometry involved will show that the size of the image will be related to the size of the object by a ratio of light-to-sound wavelengths multiplied by the dimensions of the inscnified object. This scale factor applies in the plane used for this discussion. The problem is more complicated in other planes but the basic principle still applies so that imaging can still be explained by this simple viewpoint. However, the scale factor for the relation between object and image in the other direction is unity rather than the demagnification factor expressed by light-to-sound wavelength ratio.

A careful comparison of the geometry for Raman-Nath imaging with Bragg imaging will show that the major difference is the relation between object and image orientation. For example, in Bragg imaging the images of a linear object (similar to that in Figure 5) will be oriented at right angles to the object. In Raman-Nath imaging, the object and image are not oriented exactly at right angles with respect to one another but miss this condition by arcsin λ/Λ. The difference is insignificant

in cases where water is the active medium since the ratio of light-to-sound wavelength is quite small at even the shortest sound wavelength of interest in water.

2.2 System Resolution

The highest quality images depend upon the formation of cell illumination light into a precisely convergent pattern. Deviation from diffraction limited performance will degrade image quality in two major ways. The smallest resolvable detail will be increased and cell illumination light may tend to obscure the image. For this reason, cell illumination will be considered.

Laboratory experiments are performed by expanding and collimating the beam from a laser, as shown in Figure 1. The resulting collimated light is then converged to a line at the focus of a cylindrical lens. The amplitude distribution defining light at the line-of-focus is quickly determined by observing that the light distribution in the back focal plane is just the Fourier transform of the light distribution in the front focal plane. This identification depends upon a substitution for a spatial frequency variable of transformation, f_x, as follows[9]:

$$f_x = \frac{x_i}{\lambda f} \tag{5}$$

where x_i is the coordinate in the image plane in the direction normal to the line of focus (see Figure 5).

λ is the wavelength of cell illumination light.

f is the focal length of the lens converging cell illumination light.

Although light intensity is not always uniform across the illuminating light column, this can be achieved and is usually desired. A smooth monotonic variation of no more than about 25% over the entire width has not been observed to degrade performance significantly in most applications. We shall assume that collimated light is of uniform intensity. Cell illumination light will be considered to be a one-dimensional

situation with all variation in the direction of light convergence. This is applicable to this analysis. The Fourier transform of the light distribution in the front focal plane is given by

$$u(x) = u_o \frac{\sin \pi f_x W_1}{\pi f_x} \tag{6}$$

where f_x is the spatial frequency directed normal to the axis of symmetry for convergence of incident light.

u_o is the amplitude defining the brightness of incident collimated light.

W_1 is the maximum width of the light wedge (see Figure 6).

The amplitude distribution of light in the back focal plane is then [from Eqs. (5) and (6)]

$$u_i(x) = u_o \lambda f \frac{\sin \frac{\pi W_1}{\lambda f} x_i}{\pi x_i} \tag{7}$$

The physical distance separating the zeros in Eq. (7) define width of the light at the line of focus, measured in the x direction (Figure 5). By inspection of Eq. (7), this width is given by

$$\Delta = \frac{2\lambda f}{W_1} \tag{8}$$

The image formed by diffracted light due to a point source of sound, s, is located as indicated in Figure 6 (from Ref. 11). By inspection of Figure 6 it is clear that when the point source of sound, S, is near the light beam the image will be separated from central order light if

$$R \frac{\lambda}{\Lambda} > \frac{\lambda f}{W_1} \tag{9}$$

where W_1 is the maximum width of cell illumination light.

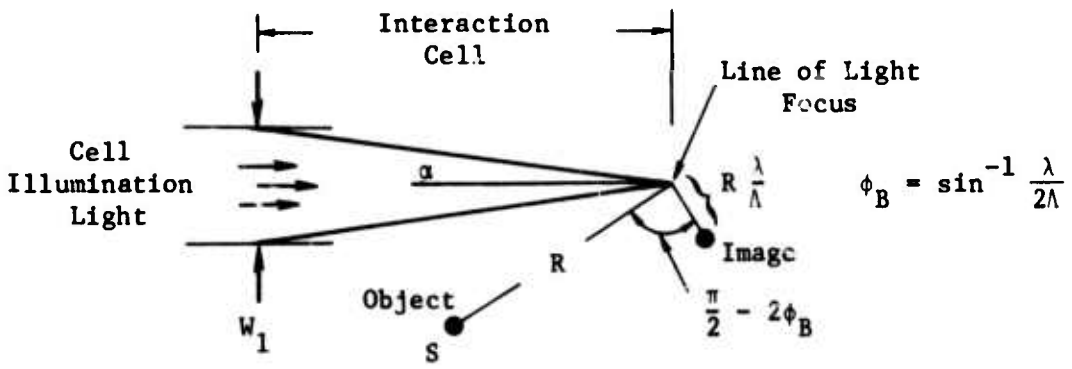

Figure 6: Image location in the acousto-optical imaging system.

For this case, a sideband image will be separated from central order light if [from Eq. (9)] (note that we have placed S near the light column)

$$R > \Lambda \frac{f}{W_1} \tag{10}$$

Assuming the image must be separated from cell illumination light, the longest sound wavelength that can be used follows from the observation that R cannot be greater than f when S is near the light column. Taking R equal to f, it follows that

$$\Lambda < W_1 \tag{11}$$

A point source of sound at a wavelength of W_1 which is located at a position most distant from the line-of-focus (R = f) but near the cell, will produce an image just to one side of the central part of the line of focus. Objects positioned more centrally must be closer to the line-of-light convergence and therefore produce diffracted light images that will be obscured by undiffracted light.

Many resolution cells are required in the field of view to form a good image. In the direction considered here, each resolution cell in the sideband image is given by the Rayleigh resolution formula for one-dimensional imaging (applied to light) as follows:

$$\delta = \frac{\lambda}{2 \sin \alpha} \approx \frac{\lambda f}{W_1} \tag{12}$$

By inspection of Figure 6, the maximum width of the image field is given by

$$W_2 = f \frac{\lambda}{\Lambda} \tag{13}$$

The total number of one-dimensional resolution cells in one direction is given by

$$N_h = \frac{W_2}{\delta} = \frac{W_1}{\Lambda} \tag{14}$$

Equation (14) states that the maximum number of resolution cells in the sound field measured in the linear direction of light convergence (left to right in Figure 6) is equal to the width of collimated light illuminating the cell, W_1, expressed in wavelengths of sound.

Equations (5) through (14) apply when the object viewed is adjacent to cell illumination light. Undersea viewing applications place the sound source at a distance from the Bragg cell. Reference to Figure 6 shows that the image will shift from the line of focus in the direction nearly aligned with propagation vectors describing cell illumination light as the sound source is moved more distance. This image movement is beyond the line-of-focus. The light is divergent in this region and tends to obscure the image formed by diffracted light. An object in the sound field positioned opposite the line-of-focus will produce an image in central order light at any object range. To keep the image out of central order light, as range to the object is increased, object position must be moved in the general direction opposite the direction

of light convergence. Figure 7 shows the field of view based on this consideration and imaging principles together with the relation between object and image positions, coupled with a geometric optical description of central order light. Objects located in the field of view shown in Figure 7 produce first order sidebands accessible without the obscuring effect of central order light even when the object viewed is at a great distance.

2.3 Working Principles of Optical Heterodyning in Acousto-Optical Imaging

System sensitivity is more universal as a range limiting parameter than resolution but not always the dominant parameter. The most sensitive system requires photosensing of the sideband image rather than direct viewing. Optical heterodyning is the basis for the most sensitive laser detector and optical heterodyning provides a way to retain doppler information in sound reflected from the object viewed. In addition, a double frequency optical heterodyning scheme has been conceived which gives the system wave arrival direction discrimination. Sound originating within a supporting vessel and moving outward can be separated from sound at the same frequency which arrives from the object viewed.

Sensitivity of an acousto-optical system tends to increase with laser power because the diffracted light intensity at a given sound level increases with laser power. The advantage of increased laser light intensity is not always obtained due to light scattered from dust particles and component surfaces. In directly viewed systems this light limits system sensitivity by the simple mechanism that the sound level must be sufficient to diffract more light than background light due to random scatter sources. By using light heterodyning an image produced by very low sound levels can be sensed even when it is completely obscured from direct viewing.

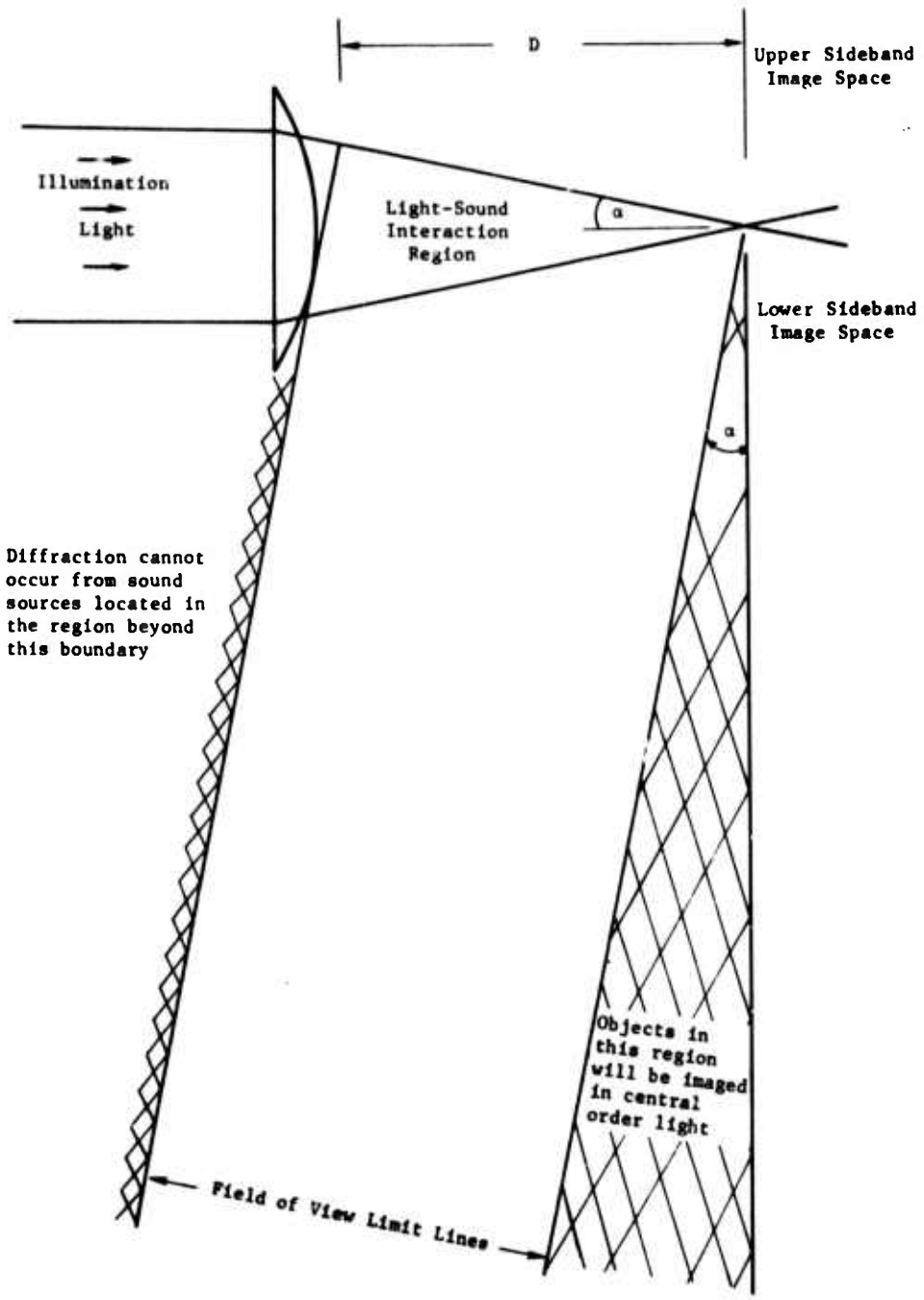

Figure 7: Maximum field-of-view for separation of the image from central order light for laboratory experiments.

The sound field defining the acoustic image to be viewed can be written

$$S(x,y,t) = A(x,y)\, e^{j\theta_1(x,y)}\, e^{j\Omega_1 t} \tag{15}$$

This expression will be considered to define sound reflected from the object viewed when the reflection mode is used.

The sound field defined by Eq. (15) interacts with cell illumination light by diffraction due to sound. This diffracted light forms two images (called sidebands) either side of cell illumination light (as already described). These images are anamorphic in the sense that magnification in the direction almost parallel to the direction of sound wave propagation is reduced by the ratio of light to sound wavelengths, but not in the orthogonal direction (normal to the paper in Figure 8). One of the sideband images is selected for viewing. For illustration, we shall select the down converted image. Light passing through the anamorphascope in Figure 8 is directed (often through additional lenses) to a plane where the image is to be sensed. Light falling on this image plane can be written (assuming unity magnification overall)

$$\begin{aligned} U_I = {} & b\, A(x,y)\, e^{j\phi_1(x,y)}\, e^{-j(w - \Omega_1)t} \\ & + N(x,y)\, e^{-j\left\{wt + \phi_n(x,y)\right\}} \\ & + c\, B(x,y)\, e^{j\phi_2(x,y)}\, e^{-j(w - 2\Omega_1)t} \end{aligned} \tag{16}$$

where b and c are complex constants determined by the system. The second term on the right in Eq. (16) represents all non-Bragg diffracted extraneous light tending to obscure the desired image. Tyndall scattering from dust particles and edge diffraction from out of cell illumination light are dominant sources giving rise to the second term on the right in Eq. (16). The last term on the right can be, and usually is, made negligible (c = 0). This term represents second order Raman-Nath diffraction forming second order sideband images (see Figure 8).

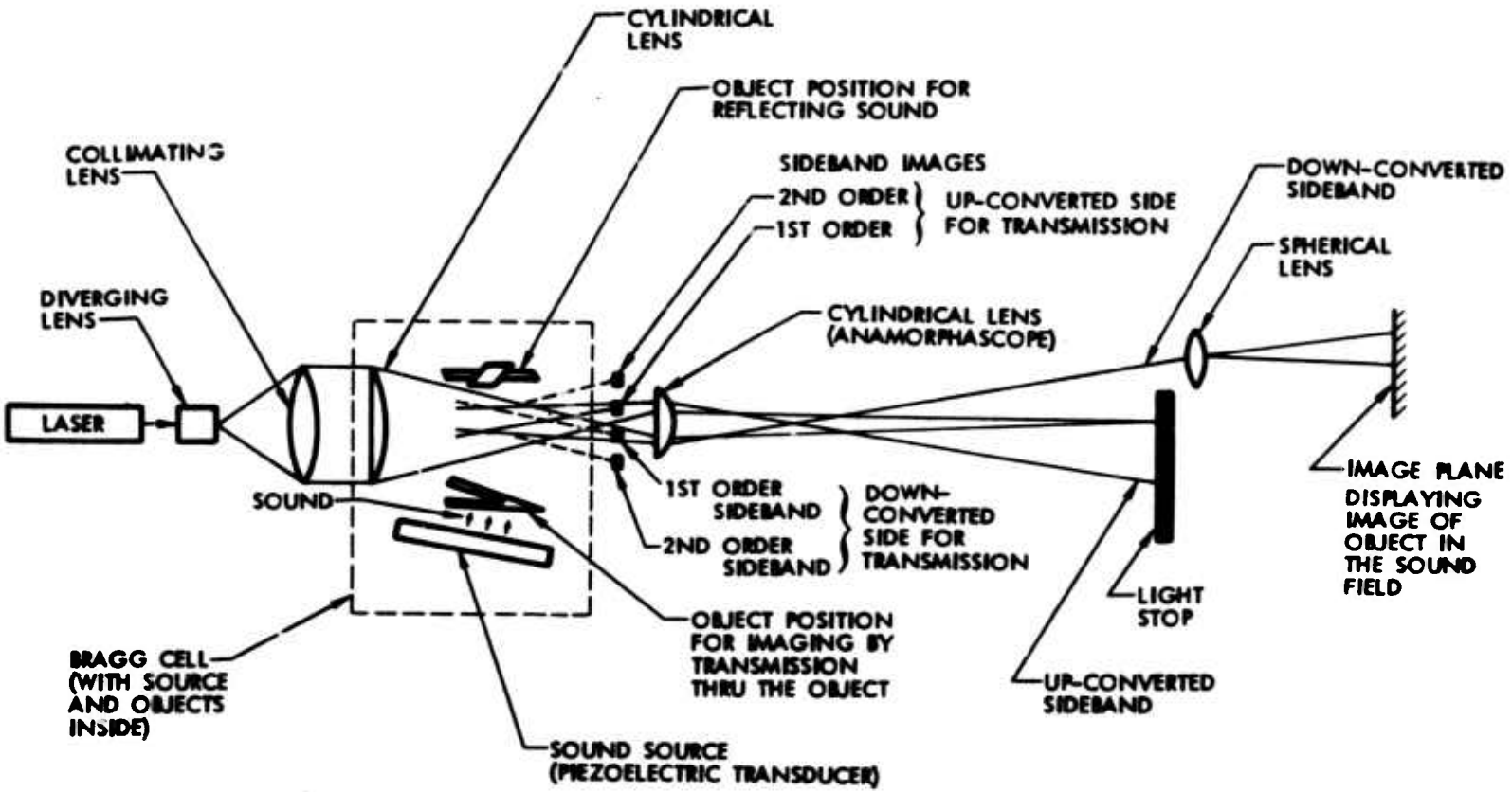

Figure 8: The TRW Acousto-Optical Imaging System for direct viewing.

The second order image is typically negligible when sound field intensities are less than tens of milliwatts per square centimeter. Additionally, the second order image will not overlap the first order image when the acoustic field of view is confined to an interval between 1/2 to 1 times the coordinate of the most distant object position where that coordinate is directed parallel to the central plane of illumination light most nearly aligned with wave vectors of incident light.

Light heterodyning makes it possible to reject all but that light which has been diffracted. This is a consequence of the shift in frequency of diffracted light which is implied by Eq. (16). (Diffracted light differs in frequency from cell illumination light by the sound frequency.) Light-heterodyning makes it possible to reject all but the narrow band of frequencies expected of light diffracted by sound.

Figure 9 illustrates the basic working principle of light-heterodyning as it applies to direct pickup of a sideband image produced by light diffraction. Figure 9 applies to the situation where the sound intensity is quite low so that only the first order sidebands are significant. The first order sidebands are represented in Figure 9 by the two arrows either side of the arrow marked ω. The frequency of the up-converted sideband is, of course, just the sum of $\omega + \Omega$. In the usual situation, both central order light and one of the sidebands will be superimposed if the frequency is low. One could therefore heterodyne a sideband with central order light without making any special provisions other than to allow superposition of both light forms. This is because the angle between the propagation direction for a sideband and for central order light is very small when the sound frequency is low. In that case, all that is necessary is to simply place a photosensor in the region where both the central order light and the sideband are

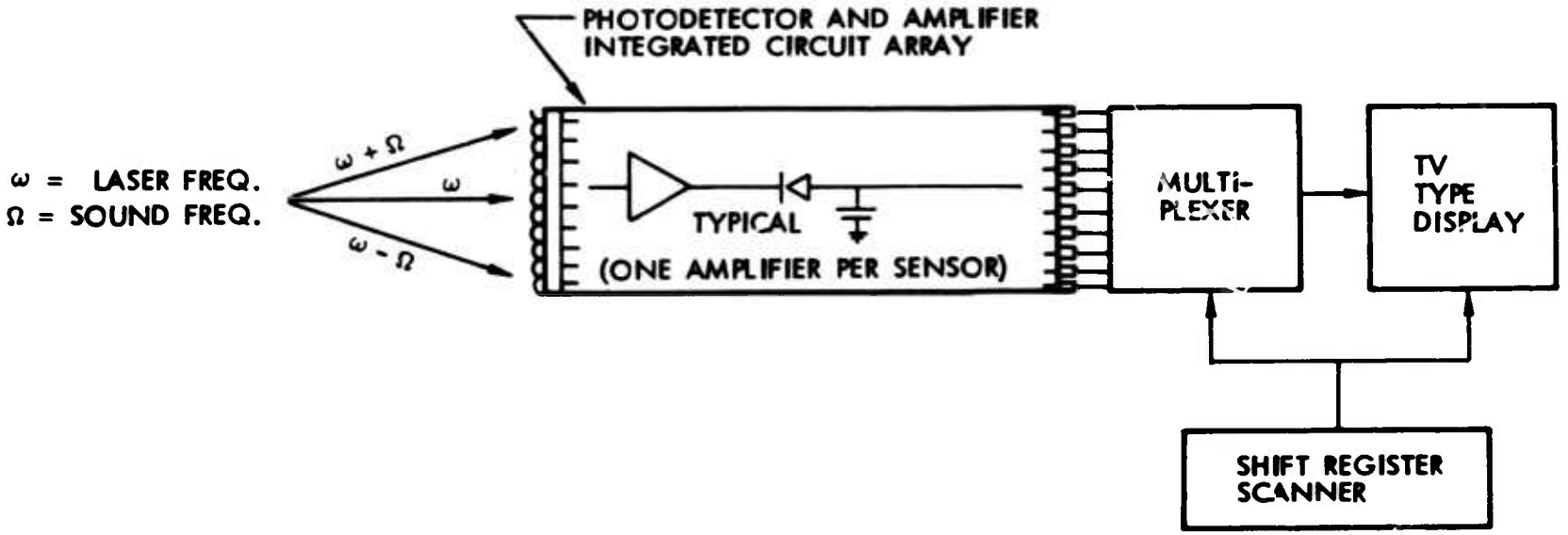

Figure 9: Working principle of heterodyne pickup for acousto-optical imaging.

present together. The desired heterodyne output, which is equal to the sound frequency, will be developed at the output of the photosensor. This will happen even for large area photosensors when the sound frequency is low, because the propagation directions of the sideband light and the central order light are so nearly parallel. Thus a major problem encountered when light-heterodyning was originally introduced[10] is no longer an obstacle.

The required parallelism is automatic in low frequency acousto-optical imaging. In principle then, all that would be necessary to use heterodyning to pick up the image would be to insert the photodetector array in the region where the sideband image will be present.

It is assumed that the photodetector array is composed of many photosensors arranged in an orderly pattern. The output from each sensor will be of amplitude in proportion to the amplitude in the sound field which is being imaged. In principal, all that would be necessary would be to pick up the output from each photodetector and replicate it in the form of light intensity modulation on a TV type display. The most sensitive system would require a different amplifier on the output of each photosensor in the array to filter and integrate the signal for subsequent sampling if the output is to be collected by the conventional sequential scan used in TV type displays. The use of a narrow-band amplifier behind each photodetector is only necessary in systems which are to possess maximum sensitivity. Fortunately, integrated circuits are now at a state of development such that it is almost a straightforward design problem to provide a separate narrow-band amplifier for each photosensor, and place this amplifier on a chip no larger than the chip required to handle the photosensors alone.

To proof test the concept, light-heterodyning experiments were performed at a sound frequency of 100 KHz. This was accomplished by simply placing a photodiode on the usual image pickup plane at the position where the sideband should appear. Output from the photodiode was amplified by a wide-band amplifier and the result displayed on a

dual channel scope. A sample of the sound source signal was also fed to the scope as a second input and both traces were synchronized to the sound source signal.

Figure 10 shows the experimental arrangement of the transducer in a top view of the Bragg cell in one test series. Here sound was simply directed (at near right angles) through convergent cell illumination light. Figure 11a shows the light-heterodyne output signal from a single light sensor (top trace). Figure 11b shows the signal across the transducer input (bottom trace). The only difference between parts (a) and (b) of Figure 11 is relative phase of heterodyne output signal (top trace). The phase is different by 180 degrees because the sound transducer was 3/4 cm farther from the light when 11b was photographed than when 11a was photographed. This demonstrates the expected phase control present in the entire system. The output from the photodiode clearly shows that harmonics are present which were not present in the sound source signal (Photodiode output was about 10 millivolts when the photographs in Figure 11 were taken.) Harmonic content is due at least

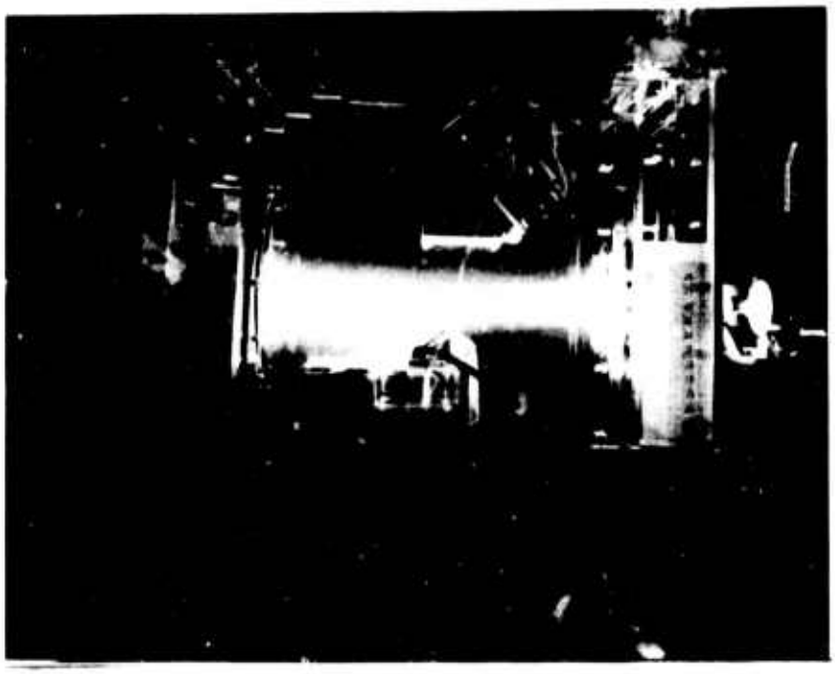

Figure 10: Experimental Bragg cell - transducer arrangement.

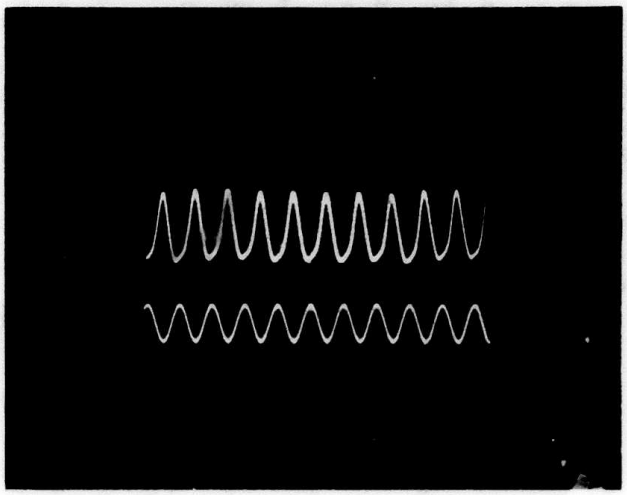

(a)

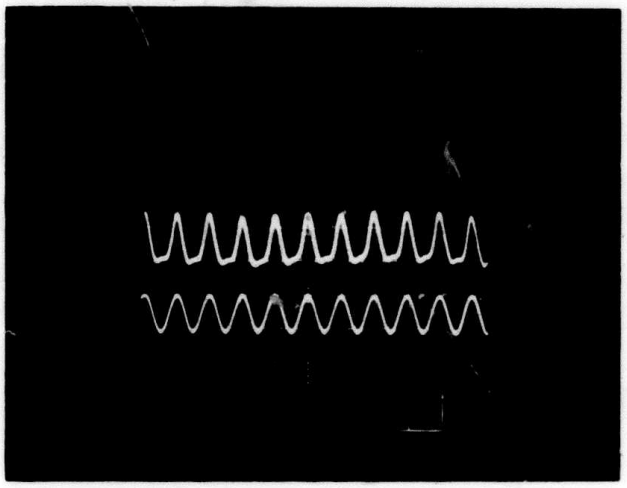

(b)

Figure 11: Light-heterodyne output signal (upper trace) compared to input transducer signal (lower trace). Note additional harmonics in photodiode output which was 10 millivolts.

in part to the nonlinear nature of open circuit output voltage of a photodiode. Harmonic content changed with diode location in the image plane. (Output current into a short circuit load is more linear.) Figure 12 shows the expected result of little or no harmonic content when the photodiode output (upper trace) was about 4 millivolts. Linear movement of the transducer changes the sound propagation path between the transducer and the light. Linear movement of the transducer always produced the expected corresponding linear phase change. The heterodyne signal went through a phase change of 360 degrees when the transducer was translated through a distance equal to one wavelength (1.5 cm at 100 KHz).

These results provide a strong indication that images can be formed from sound at frequencies of 100 KHz and lower by use of a light-heterodyne detector as the image pickup device.

A superheterodyne image sensor can be made with either a single sensor (such as the photodiode referenced above) or an array of sensors that cover the image area. The array of sensors can be an order of magnitude more sensitive than the scanned single sensor system since all light falling on the image is processed in the array. In a scanned

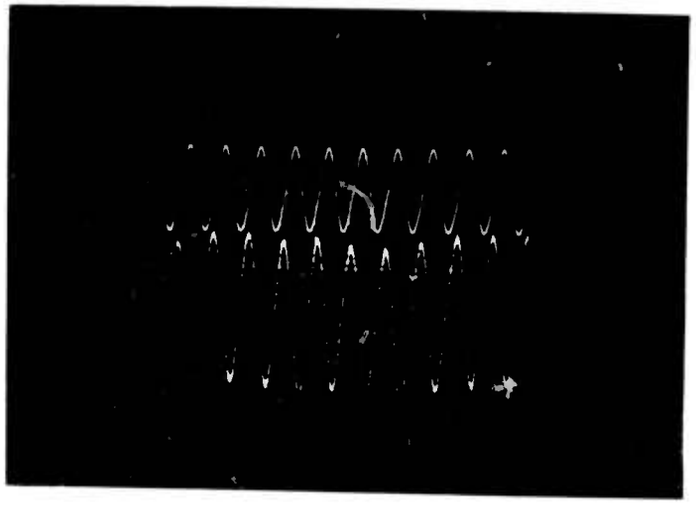

Figure 12: Light-heterodyne output signal (upper trace) compared to input transducer signal (lower trace). Note reduction in harmonic content at 4 millivolt output.

system, light falling outside the point being scanned is lost at times other than the instant the given point is scanned. Of course, the output of an array like that illustrated in Figure 9 can be scanned without loss of system sensitivity since information collected full time can be later collected sequentially by periodic sampling in a sequential manner.

A convenient method used in heterodyned imaging experiments reported here involved a scanned sensor to intensity modulate an oscilloscope. Signal from the narrow-band amplifier is rectified for the spot intensity input and the signals used to position the image sensor are used as x-y inputs to control the oscilloscope spot position.

The best approach would be to use an array of sensors capable of collecting the heterodyned signal full time. No such array, which is also suitable for heterodyning, is presently available. Such an array might be made next year by modifying a light sensitive array which was designed and built by TRW Systems Group for the U.S. Army Electronics Command in Fort Monmouth, N.J.[6]

There are many possible configurations for processing a sideband image by the light-heterodyne technique. Previous methods[10,11] have required the addition of a sample of light from the same laser by way of an external path. This light (called the reference beam) is made to have uniform intensity over the image pickup plane. Previous heterodyning methods have therefore used a reference light beam having the exact same frequency as cell illumination light. The reference beam and extraneous non-Bragg diffracted light are at the exact same frequency.

One heterodyning configuration used general background light as the local oscillator field. Here background light becomes a requirement rather than a light field which obscures the image. Figure 13 shows the results of an experiment where this was done. The object forming the sound in these experiments was a round transducer excited with sufficiently low power to allow general background light to completely obscure the image. Phase sensitive amplification is an

(a) (b)

Figure 13: Light pattern on (a) the image plane and (b) the memory scope which stored the heterodyne signal. The object producing the sound source was a single round object. The obscured image is located at the extreme right of the image plane shown in Figure 13a. Note that the scales in Figures 13a and b are not the same.

essential part of the system which was used to form the image in Figure 13b. Note that the image is completely free of background. The desired phase sensitivity has its origin in the fact that the demodulated signal from the sidebands is 90 degrees out of phase with the demodulated signal from scattered light. The lock-in amplifier is particularly convenient where it is desired to reject a signal occurring at a specific phase. The lock-in amplifier will reject a sinusoidal signal with a phase determined by a control on the amplifier. Figure 14 shows the system used to make the image in Figure 13b. In this system illumination light is modulated by an amplitude modulated 40 MHz carrier. The 40 MHz carrier is amplitude modulated by a frequency Ω_2 which is near but not equal to the sound frequency. A sideband is similarly modulated but shifted in frequency. Scattered light is of the same frequency as cell illumination light so that the frequency components in diffracted light differ from frequency components in scattered light by the frequency of the sound. Since the photosensor used would not produce an output at any frequency higher than about 2 MHz, the only signal at the detector output is at the sound frequency Ω_1, Ω_2, $\Omega_1 + \Omega_2$ and $|\Omega_1 - \Omega_2|$. Only a signal at the difference frequency $|\Omega_1 - \Omega_2|$ is amplified by using a sample of the transducer drive mixed with a sample of modulator drive to obtain $|\Omega_1 - \Omega_2|$ for the reference input on a lock-in amplifier (marked REF in Figure 14).

At low sound frequencies, cell illumination spills over onto the sideband images to greater degree as the sound frequency is lowered. At frequencies as low as 100 KHz, the intensity of this spillover may be greater than the desired intensity of the reference beam and the intensity level may not be uniform over the image. With this configuration it is therefore next to impossible to obtain an ideal uniform reference field over the image pickup surface in systems of reasonable size which operate at low frequencies.

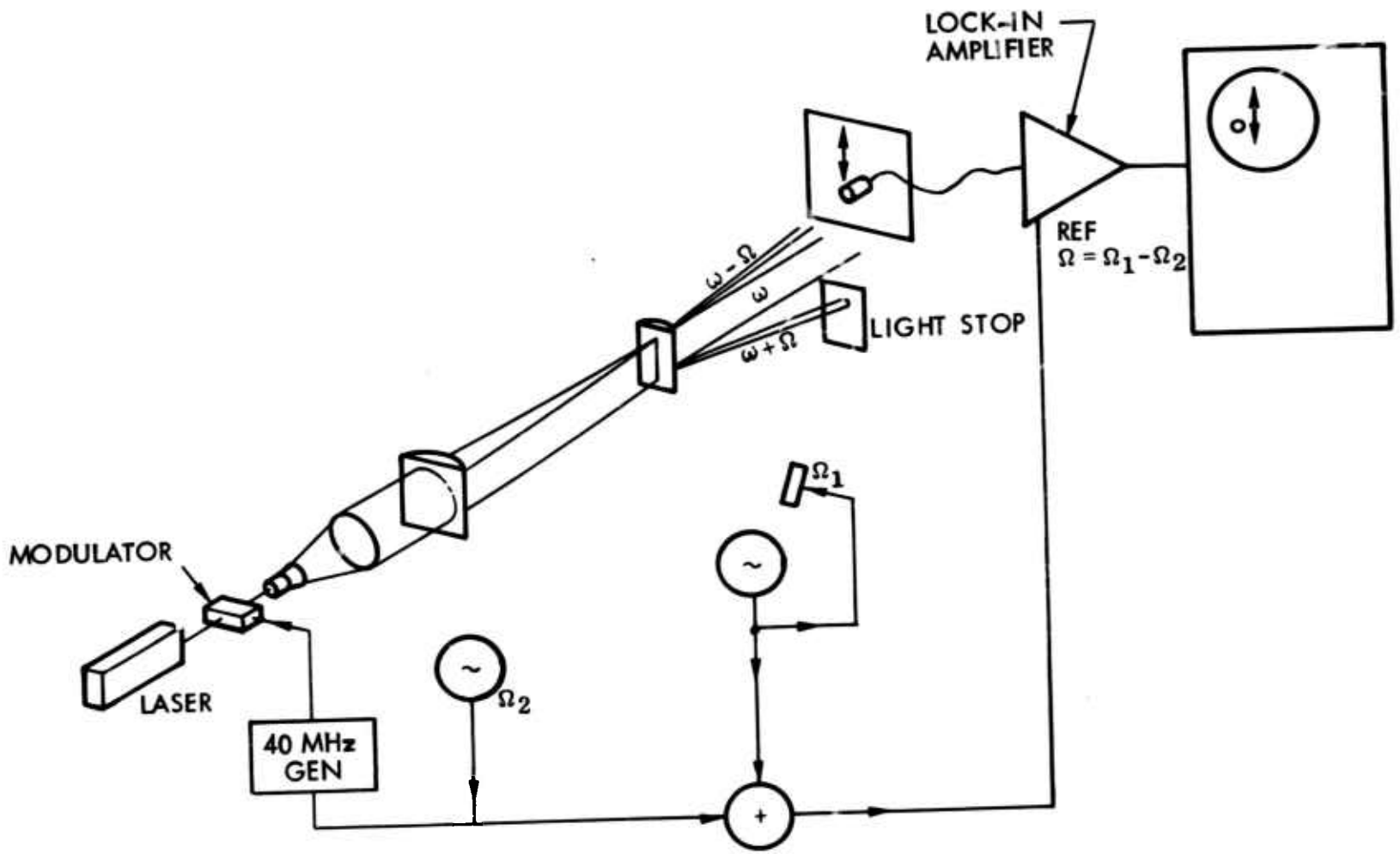

Figure 14: A light-heterodyne acousto-optical system which uses scattered light for the local oscillator wave.

A reasonably uniform and separable reference light field was obtained at a different frequency than cell illumination light by using sound to diffract a sideband image of a nearby transducer onto the image plane. This was done by forming a sideband image on the same space as the entire field containing the down-converted image of the object to be viewed. Early heterodyne experiments on this project were performed with one transducer providing both object illumination and reference beam formation (see Figure 15).

Figure 15 shows how the heterodyning signal could be formed with a uniform reference beam background. The system illustrated by Figure 15 is configured so that an upper sideband is used to provide a uniform reference field, and the lower sideband contains the image of the object to be viewed. There is only one sound transducer in this configuration. This sound transducer generates a sound wave which passes through the cell illumination light (shown in the figure as convergent from left to right). The sound transducer is imaged in sidebands one on each side of cell illumination light. Consider the up-converted image of the transducer. Sound from the transducer, which passes through cell illumination, is reflected by the object to be viewed and returns to cell illumination light. This reflected sound also forms two sideband images. Consider the down-converted image due to reflected sound. Note that the down-converted image, due to reflected sound, can be superimposed on the up-converted image from the sound source transducer. The sound source transducer produces a uniform field. It is therefore an ideal reference field for heterodyning with the image replicating the object to be viewed. This is the situation for the system shown in Figure 15. The photosensor array would be made of sufficient size to cover the entire image which exists in the orthoscopic plane shown at the extreme right.

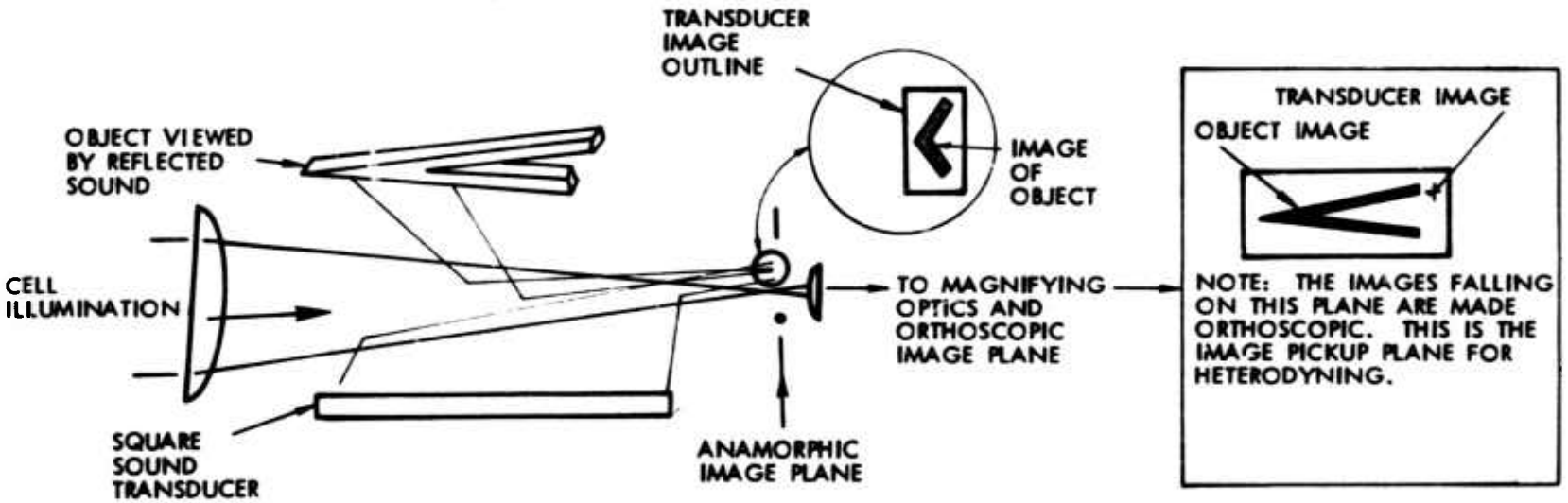

Figure 15: Geometry for heterodyne pickup of a sideband image.

When one transducer is used to form the reference field and also illuminates the object (as in Figure 15) the transducer forms the desired up-converted image, light forming a uniform image of the transducer can be expressed by

$$U_R = u_o e^{j\theta(x,y)} \; e^{-j(w + \Omega)t} \tag{17}$$

The amplitude of the light field falling on the final image plane is just the sum of Eqs. (16) plus (17). Almost all photosensors produce an output signal which is proportional to intensity. Light-heterodyning consists of superimposing two light fields on a sensor responding in direct proportion to intensity. The desired heterodyne output signal is thus derived from light intensity falling on the sensor. Calculating the resulting intensity on the image plane, we obtain

$$\begin{aligned} I = \frac{1}{2}\left[b^2A^2 + N^2 + U_o^{\,2} + c^2B^2\right] \\ + \frac{1}{2}\Big\{ bAN \cos(\Omega_1 t + \phi_1 - \phi_n) \\ + bAU_o \cos(2\Omega_1 t + \phi_1 - \theta) \\ + NU_o \cos(\Omega_1 t + \phi_n - \theta) \\ + c\,baB \cos(\Omega_1 t + \phi_2 - \phi_1) \\ + c\,BN \cos(2\Omega_1 t + \phi_2 - \phi_n) \\ + c\,BU_o \cos(3\Omega_1 t + \phi_2 - \theta)\Big\} \end{aligned} \tag{18}$$

(Arguments previously shown for A, B, ϕ_1, ϕ_2 and θ are not shown for simplicity of exposition.)

Output from the heterodyne sensor may therefore contain the sound frequency plus its first and second harmonic. As noted before, c can be made equal to zero. When c = 0, only one term is at twice the frequency of the sound and this term is given by

$$U_s = \frac{1}{2} U_o bA(x,y) \cos(2\Omega_1 t + \phi_1 - \theta) \tag{19}$$

The amplitude of the expression in Eq. (19) is proportional to the the sound field in Eq. (15). If U_o is uniform over the pickup image plane (as assumed), then a good image of an object in the sound field is obtained by rejecting all signals implied by Eq. (18) except for the term given by Eq. (19). This is easily done by amplifying the sensor output with a narrow-band amplifier tuned to twice the sound frequency.

Second harmonics will be generated when the transducer for object illumination is driven at maximum possible intensity. An interfering background has been observed when this is the case, and c in Eq. (18) cannot be assumed to be zero. Fortunately, this problem is easily overcome by using a signal at a different frequency to energize a second nearby transducer. The frequency selected for the sound used for object illumination will typically be made much less than the frequency of the signal used to energize a low power transducer used to form the uniform reference field needed for heterodyning. This variation is illustrated in Figure 16.

2.4 Two Frequency Bragg Imaging System

The imaging system described above can be improved and made more flexible by the modification shown in Figure 16. One problem encountered with the previous system was that second harmonics were generated by nonlinearities when the sound level was increased sufficiently to see a small object. This produced a background obscuring the image. A second and important advantage of this system is that the signal frequency out of the photosensor can be made several orders of magnitude less than the sound frequency. An array of low frequency amplifiers can be made as an integrated circuit. This is nearly impossible at high frequencies. The following system completely removes this problem. It has been tested experimentally under this contract.

Either the transmission mode or reflected mode is assumed to produce sound at frequency Ω_S. This is made to form the usual sideband image of the object. A second transducer, the reference transducer, generates a sound field at frequency Ω_R. The reference transducer is

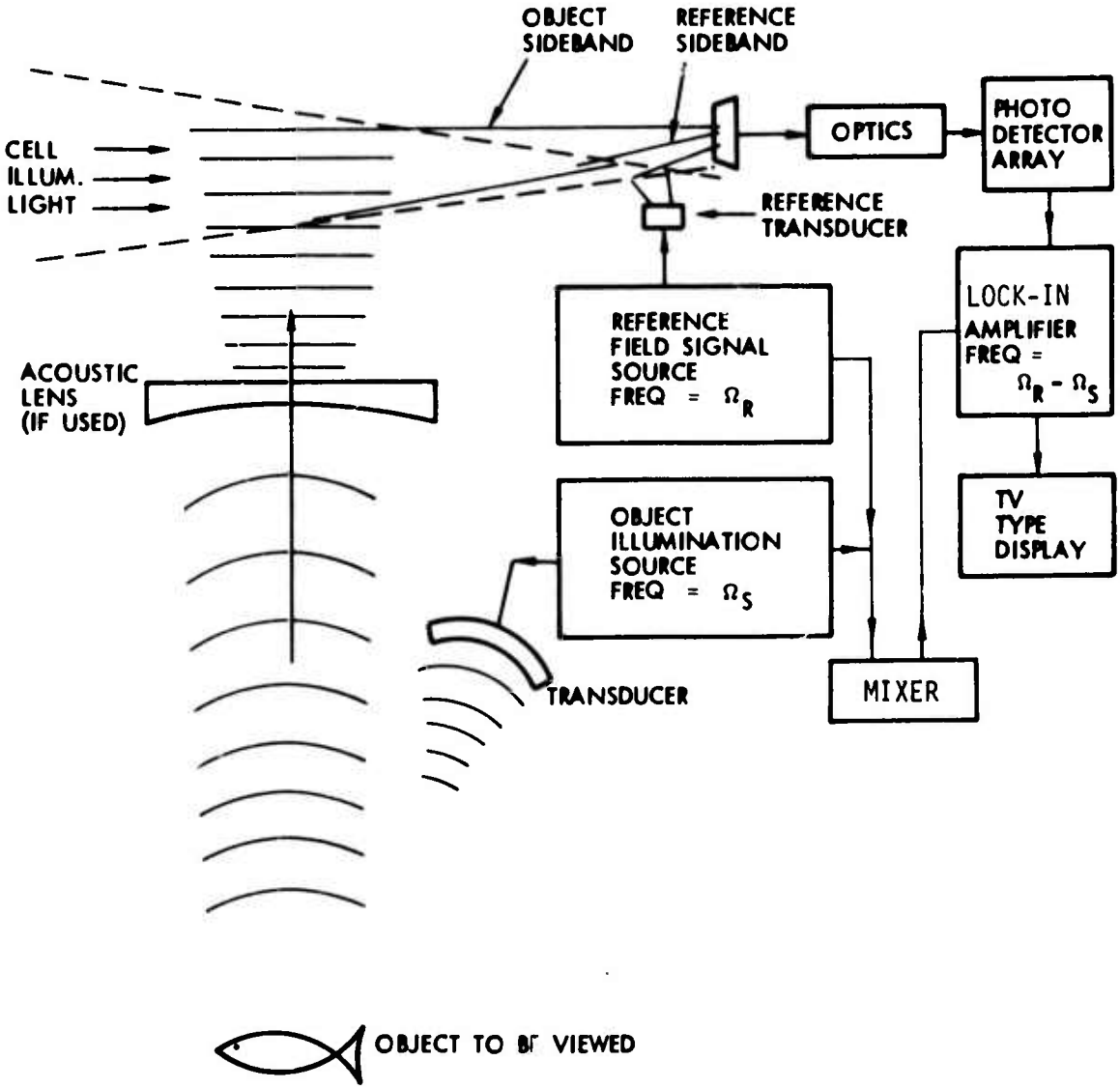

Figure 16: A double frequency heterodyning acousto-optical imaging system.

positioned to form an image covering the field of view outlined in the image plane used to view the object. Thus a light field at frequency $w - \Omega_S$ forms an image of the object. On the same plane there is also an image of the transducer; this image is just a uniform field of frequency $w - \Omega_R$ when the pictured configuration is used. Since only the difference frequency results from light heterodyning, the desired signal out of the photosensor is at the frequency $\Omega_R - \Omega_S$. The frequency Ω_R must be greater than Ω_S if the relative transducer positions are as shown in Figure 16. A narrow-band amplifier tuned to $\Omega_R - \Omega_S$ amplifies only the desired signal.

This technique has also been implemented with the reference transducer and object viewed on opposite sides of the light column. The main difference is that here the frequency of diffracted light forming one of the two images will be equal to the sum of the respective sound frequency and incident light frequency, whereas light forming the other image would be a frequency equal to the incident light frequency minus the respective sound frequency. The desired heterodyne output frequency is therefore either $|W + \Omega_R - (W - \Omega_S)|$ or $|W - \Omega_R - (W + \Omega_S)|$ and both of these expressions equal $\Omega_R + \Omega_S$. The desired heterodyne output frequency is equal to the sum of the respective sound frequencies when the object and reference transducer are placed on opposite sides of the cell illumination light column.

2.5 Low Frequency Imaging by Heterodyning in Central Order Light

It is possible to form an image within central order light where sideband light is not involved. This can be understood from the observation that light diffracted into both sidebands has the effect of superimposing a modulation on cell illumination light. Removal of light at the frequency of one sideband must place a similar signal at the same frequency on central order light. The modulation impressed on central order light by removal of both Raman-Nath sidebands is such that recombination into the original form will return central order light to its

original unmodulated state. After light has been diffracted away from unmodulated cell illumination light into two sidebands, remaining central order light may be described as composed of a carrier plus two temporal sidebands. The meaning of the word "sideband" as used in this paragraph is the same as common usage in communications systems. Only sound wave components with planes of constant phase aligned with an encountered light ray produce diffracted light. Image that can be sensed by a photodetector is therefore impressed upon central order light in much the same way as the formation of images in the sidebands.

This has been demonstrated experimentally on this contract by using an acoustic lens to convert spherically divergent sound waves to cylindrically convergent waves in the light-sound interaction region. More specifically, horizontally divergent rays are made plane while maintaining imaging in the other (vertical) direction. Thus, sound from any point on an object is converted to a plane wave by an acoustic lens. The orientation of the phase front of this plane wave will vary with source point position (on the other side of the acoustic lens). Diffraction due to this plane wave of sound will only apply to a unique columnar light ray. This ray will produce a heterodyne signal. The horizontal variation in the image is formed in this way. Vertical variation is as it has been. The object must be at any imaging location for vertical detail while it must be at the focus of an acoustic lens for detail that varies with horizontal position. Two cylindrical acoustic lenses are needed for long distance large field viewing. If they are at the same location, they must have different focal lengths. The lens with the power direction horizontal will be at a focal distance from the Bragg cell. The objective of this lens is to form the Fourier transformation of sound field existing at the object viewed. In the above, the cylindrically convergent light column is assumed to be oriented with the axis of the line-of-focus vertical (as it is in our lab).

Central order light, processed in this way, was caused to fall on an image plane. This plane appeared to be uniformly illuminated to the naked eye. A photosensor was scanned over the image plane illuminated by expanded central order light. The sensed heterodyned signal was observed to possess image qualities. However, no attempt was made to form quality images in this manner since it was done at a frequency of about 100 KHz and too few resolution cells were present in the image to reproduce detail. A much larger width for cell illumination light is required to obtain sufficient image detail to form quality images.

3.0 LABORATORY RESULTS

3.1 Summary of Experiments

Laboratory experiments to determine the feasibility of low frequency image formation have been performed. These experiments were directed at verifying theory and determining practical limitations that would be encountered in the process of constructing an imaging sonar. Resolution, system sensitivity, and field of view were the main parameters of interest. These characteristics were checked experimentally under a variety of conditions. Applicable conditions included range between the acousto-optical cell and the object viewed, sound frequency and dimensions of the cell.

Figure 4, presented early in this report, showed an example of images which were formed from sound reflected by a small object at a distance of 15 feet from the acousto-optical cell. A smaller object was imaged at a frequency of 1.8 MHz with the same system. This object was also shaped like a submarine, as shown in Figure 17. Figure 17 shows that the image obtained at this frequency is quite good. Resolution of the system at 1.8 MHz is less than 1/2 cm in the horizontal direction. Images in Figures 4 and 17 were obtained with the acoustic lens in front of the 4-foot cell as shown in Figure 2.

Near point sources were used in resolution experiments performed to obtain stated results below. Resolution was determined by using two identical transducers separated by the smallest distance at which the two transducers could be distinguished as different than an image of just one transducer. These experiments showed that theory defined resolution of our system with an accuracy of at least one-half at a frequency on the order of one megahertz. Theory and experiment differed by almost an order of magnitude at frequencies of 500 KHz and below. This discrepancy may be due to the fact that less than 20 wavelengths of sound fit within the width dimension of the light-sound interaction region at the lower frequencies.

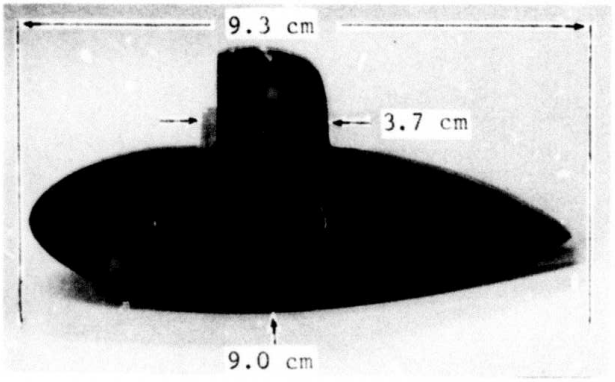

OBJECT USED IN 1.8 MHz IMAGING.

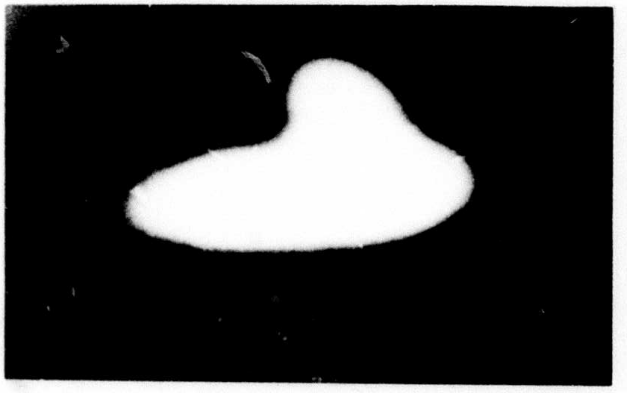

IMAGE OF THE OBJECT AT 1.8 MHz.

Figure 17: Images formed at 1.8 MHz in the TRW Bragg Imaging System with sound reflected from object at a distance of 15 feet.

A second series of experiments were performed to determine the maximum sensitivity that would be available in the TRW Acousto-Optical Imaging System. Sensitivity was obtained by using a photomultiplier driving a lock-in amplifier with phase sensitive response. The lock-in amplifier approach to narrow-band amplification is particularly convenient for use in an integrated circuit because it is digital in nature and requires no inductors for obtaining the required narrow-band pass characteristic.

3.2 Sensitivity Measurements

Sensitivity of the system shown in Figure 14 was measured by directing image light to a photomultiplier. The results are shown in Figure 18. These are expressed in terms of sound level to produce a unity signal-to-noise ratio. In making these measurements, a small sound source was placed at a distance of 15 feet to allow sound to become more planar over most of the 4-foot length of the light-sound interaction region. Sound level was determined using the expression in Appendix A and transducer electrical power input. A cylindrical acoustic lens was used to confine all sound to arrival within the 6-inch high column of cell illumination light.

3.3 Resolution Measurements

The TRW Acousto-Optical Imaging System, utilizing the 4-foot (1.22 meter) interaction cell shown in Figure 2, was used to determine system resolution at low frequencies. The frequencies used were such that the number of sound wavelengths that fit within the light wedge are too few to consider diffraction to precisely fit Raman-Nath (or Bragg) assumptions in all cases. Resolution measurements were made with the object transducers adjacent to the light-sound interaction region. Resolution measurements were also made with the object transducers 15 feet from the light-sound interaction region.

Resolution in directions aligned with the axis of light convergence is determined by the cylindrical acoustic lens at the low frequencies used here. Resolution in the orthogonal direction is determined by the

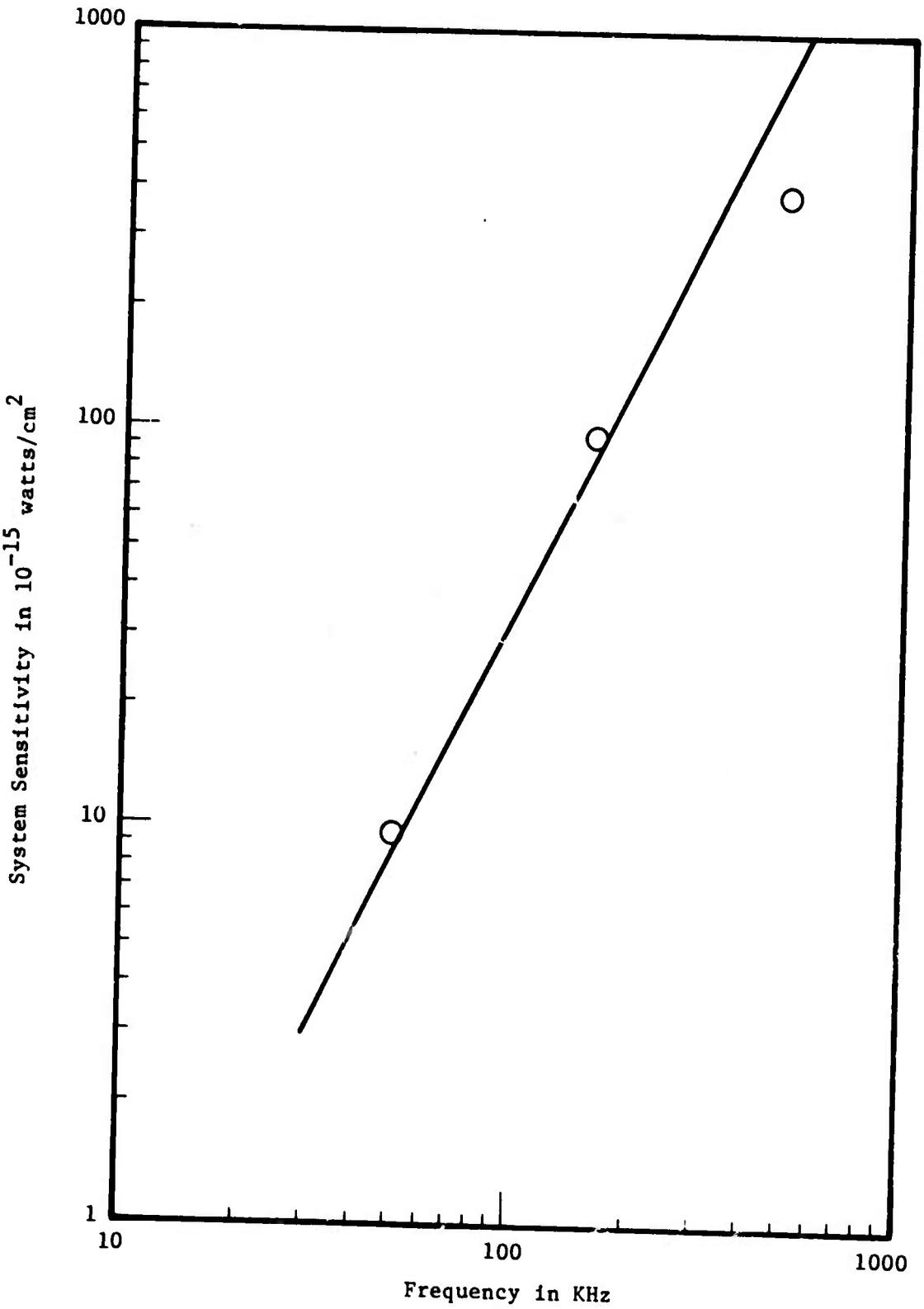

Figure 18: System sensitivity as a function of frequency.

light-sound interaction. When the object is close to the light-sound interaction region, resolution measured in the plane of light convergence is given by[12]

$$\delta = \Lambda/2 \sin \alpha \tag{20}$$

where Λ = the wavelength of the sound involved

2α = the wedge angle of the light column

R = the range of the object to the first acoustic lens or the interaction cell if no acoustic lens is present

D = the maximum extent of the aperture which collects sound scattered by the object

When the object is at a great distance, resolution is given by

$$\delta = \Lambda \, R/D \tag{21}$$

The region where Eq. (20) is applicable is the region where the horizontal angular extent of the light field limits the maximum horizontal directed spatial frequency that contributes to image formation. At greater ranges more light is present than can be used because the horizontal width of the aperture limits the angular extent of captured sound waves to a smaller interval than the maximum angular extent of cell illumination light. The cross-over point of the applicable regions for each expression is

$$\lambda/2 \sin \alpha = \lambda R/D \quad \text{or}$$

$$R = \frac{D}{2 \sin \alpha} \tag{22}$$

The region at a range less than the value given by Eq. (22) will be referred to as the light limited region. The region at a range greater than that given in Eq. (22) will be referred to as the aperture limited region.

A schematic diagram defining the first experiments in the 4-foot acousto-optical imaging system is shown in Figure 19. Photographs of the actual optical components and object transducers are shown in Figure 20.

These figures show the optical components of the preliminary 4-foot interaction cell acousto-optical imaging system. The light beam forming optics include a beam expander consisting of a spatial filter with an 8.5 mm focal length lens and a 6.8 μm aperture. This spatial filter fills a collimating lens (544.5 mm focal length by 159 mm diameter) located 50 cm away. The collimating lens forms a parallel beam which falls upon the interaction cell entrance window at a distance of 91.5 cm. Between the entrance and exit windows at one end of the tank, the light wedge is formed by a cylindrical lens (300 mm focal length) located 7.6 cm inside. The tank is 18 feet (5.99 meters) long, 4 feet (1.22 meters) wide in the direction of incident light and 3 feet (.91 meters) deep (normal to the paper in Figure 19). Part of the tank is occupied by a skimming, filtering and recirculating system limiting the usable length to 15 feet. With the aid of an acoustic lens, sound from 15 feet away is focused within cell illumination light. Resulting sideband images are magnified by a second cylindrical lens (22 mm focal length) located 37 cm from the exit window. A mirror 64 cm away reflects the image onto a converging lens (544.5 mm focal length) at a distance of 57 cm. A third cylindrical lens (305 mm focal length), 76.2 cm away is oriented horizontally and used to control the vertical magnification. A fourth cylindrical lens (22 mm focal length) located 43.2 cm from the third cylindrical lens increased the horizontal magnification. The image was focused onto an image plane at a distance of 368 cm. The angle α in this configuration was .967°. The light limited region extends to a distance for this configuration of $R = 36.1$ meters.

Resolution measurements consisted of observing the two object transducers. The two light spots forming the image were then made to

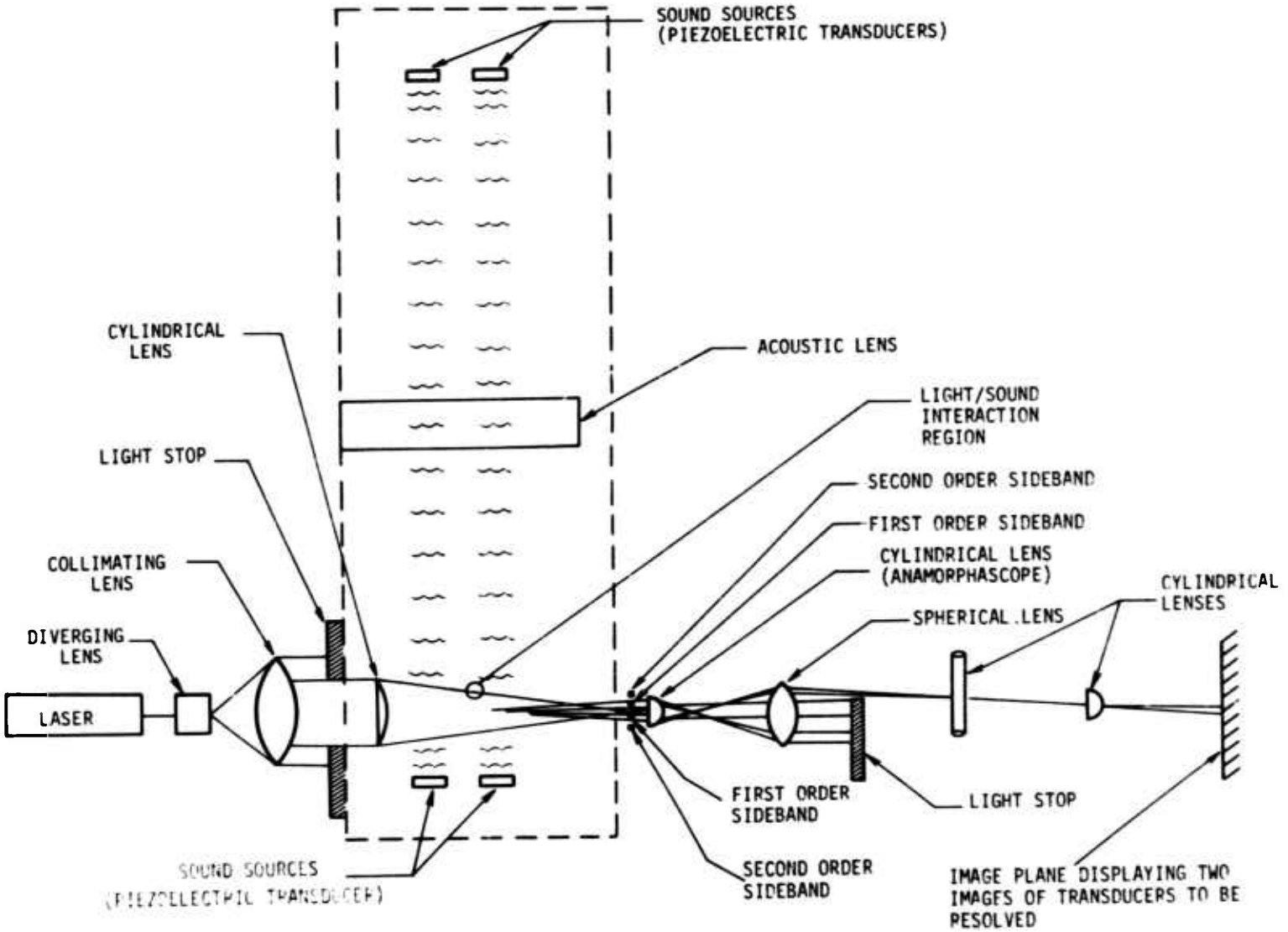

Figure 19: First four-foot interaction cell acousto-optical imaging system.

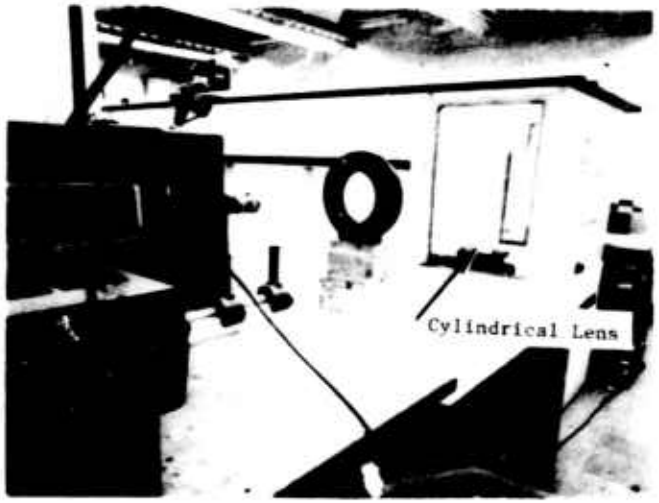

(a) Light wedge forming optics including interaction cell entrance window.

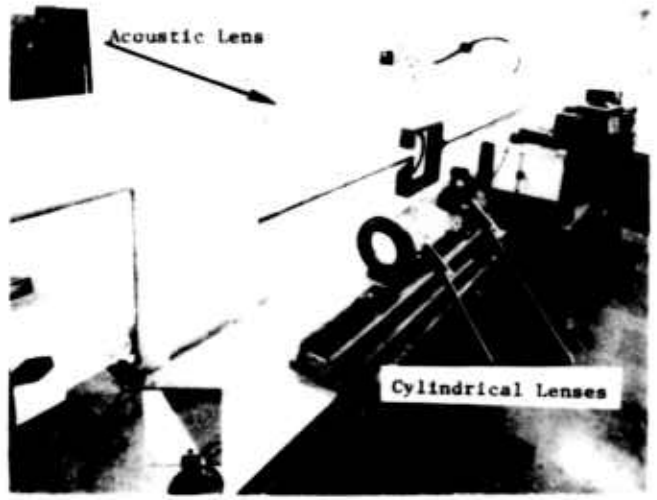

(b) Imaging optics including interaction cell exit window.

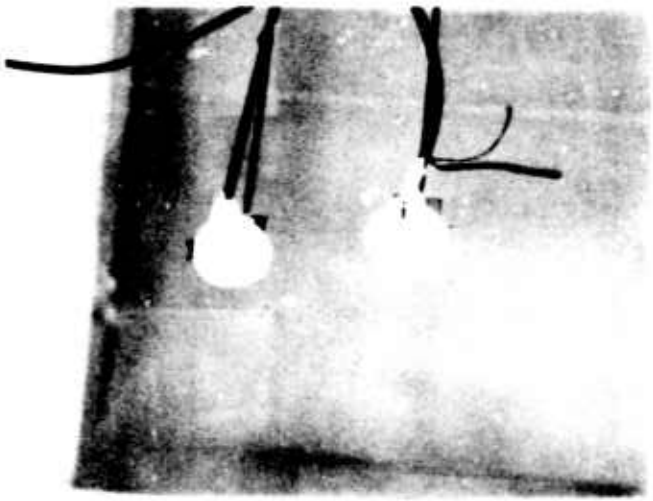

(c) Object transducers used for resolution measurements.

Figure 20: Optics of the first four foot acousto-optical imaging system and object transducers used for resolution measurements.

approach one another by moving the object transducers together until a minimum clear separation was obtained. The distance between the two transducers was then measured and recorded as the acousto-optical imaging system resolution. Two types of measurements were made. The first measurements were made with the object transducers at different elevations. This will be referred to as "off-axis". Off-axis measurements were made by placing one transducer over the other so that they appeared as two spots, one over the other. One of the two transducers was shifted horizontally just enough to form an image such that no vertical line would pass through the image of both transducers (see Figure 21). Physical separation of these transducers was then measured and recorded. The second measurements were made with the transducers side-by-side at the same elevation. This will be referred to as "on-axis". Representative photographs with transducers next to the light column are shown in Figure 21. Figures 21a and 21b contain transducer images at 830 KHz for the off-axis case. Measurements with on-axis configurations (shown in Figures 21c and d) were made by recording the smallest separation distance producing two spots. The slanted appearance in Figure 21b would appear vertical when the anamorphascope is correctly aligned. The horizontal magnification in this system makes a very slight tilt of the anamorphascope result in a marked tilt in an image.

The frequencies used for measurements at 15 feet were 830 KHz and 500 KHz. Typical photographs are presented in Figure 22. Figures 22a and 22b contain transducer images at 830 KHz for the off-axis and on-axis configurations, respectively. Transducer images at 500 KHz for the off-axis and on-axis configurations are shown in Figures 22c and 22d, respectively. Minimum observed separation distances are given in Table I.

A second series of resolution measurements were taken with a larger wedge angle for cell illumination light. As shown in Figure 23, the interaction beam which was formed with a 25.4 cm cylindrical lens

(a) Images of two off-axis transducers at 330 KHz.

(b) Images of two on-axis transducers at 830 KHz.

(c) Images of two off-axis transducers at 160 KHz.

(d) Central order image pattern for no sound

Figure 21: Images formed with two object transducers next to the light column and close together using the first four-foot interaction cell.

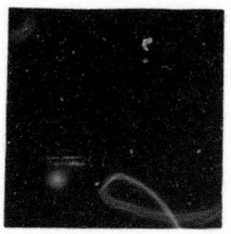

(a) Images of two off-axis transducers at 830 KHz.

(b) Images of two on-axis transducers at 830 KHz.

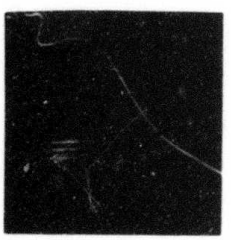

(c) Images of two off-axis transducers at 500 KHz.

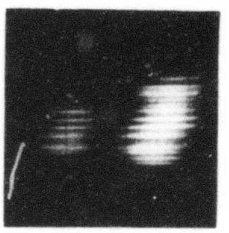

(d) Images of two on-axis transducers at 500 KHz.

Figure 22: Images of two transducers at a distance of 15 feet and separated by a resolution distance using the first four-foot interaction cell.

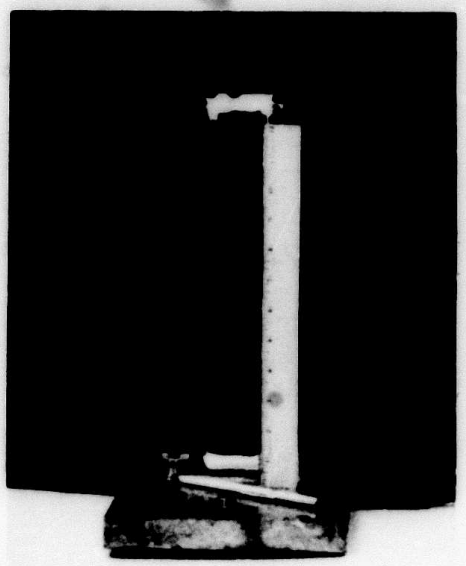

(a) 5.1 cm cylindrical lens used in the first four foot acousto-optical imaging system.

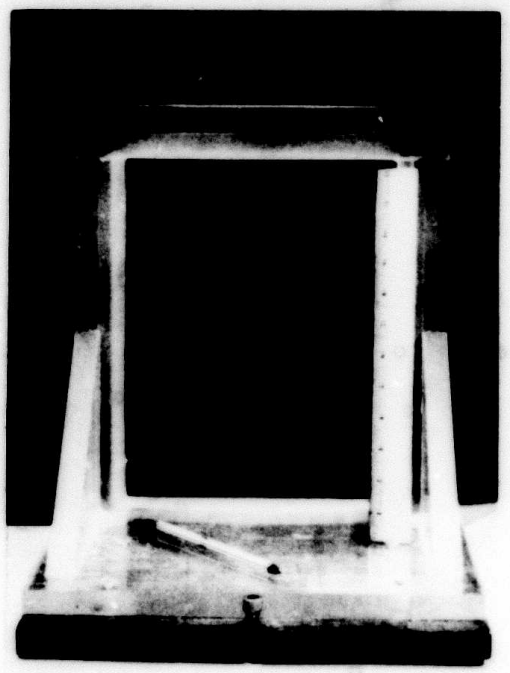

(b) 25.4 cm cylindrical lens used to replace the 5.1 cm lens above.

Figure 23: Optical components of the four foot acousto-optical imaging system.

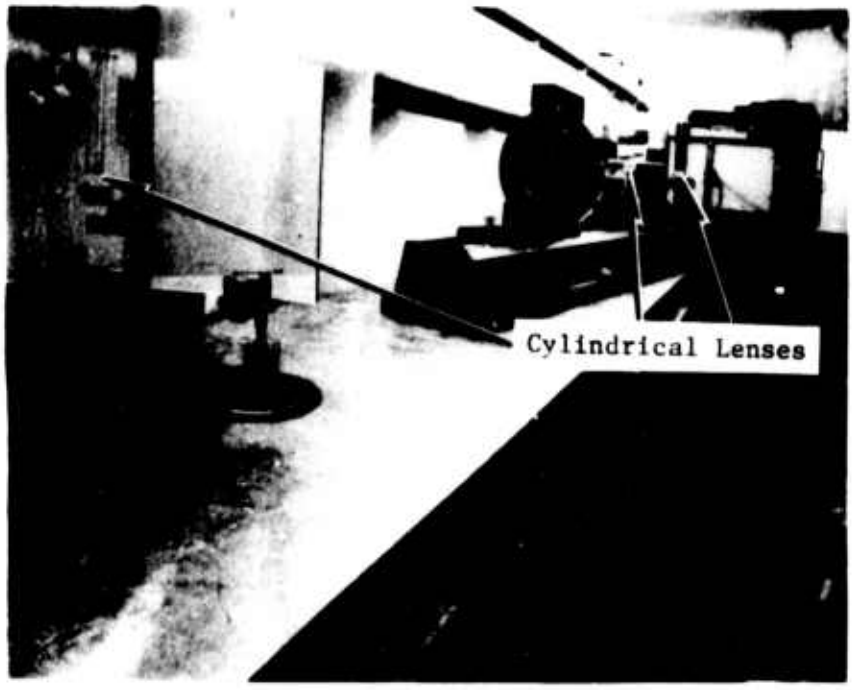

(c) Optical train for imaging formation.

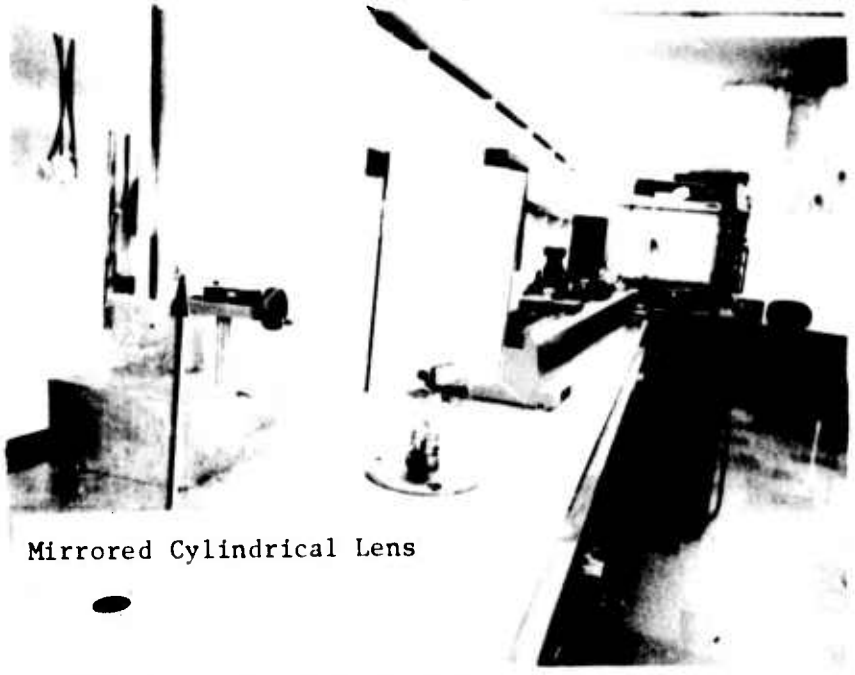

(d) Mirrored cylindrical lens system replaces the lenses in part (c).

Figure 23: Optical components of the four foot acousto-optical imaging system.

Table I: Resolution measurements for the first four foot (1.22 meter) Bragg cell acousto-optical imaging system.

Frequency	Transducers Off Axis*	Measured Resolution Transducers On Axis	$\Lambda/2 \sin \alpha$
	OBJECTS NEARBY		
1.18 MHz	3.9 cm	15.3 cm	3.9 cm
830 KHz	5.1 cm	15.3 cm	5.4 cm
500 KHz	8.9 cm	19.1 cm	9.0 cm
160 KHz	45.2 cm	57.2 cm	27.1 cm
111 KHz	47.7 cm	67.5 cm	40.5 cm
	OBJECTS AT 15 FEET		
830 KHz	14.0 cm	14.0 cm	5.4 cm
500 KHz	15.3 cm	19.3 cm	9.0 cm

* Transducer separation when the image appeared as in Figures 21a and c and 22a and c.

which replaced the 5.1 cm wide lens. This change improves the resolution capabilities when the object is in the light limited region,* but resolution in the aperture limited region remains the same. The light limited region extends out to R = 4.6 meters. Although resolution is not improved by changes in the anamorphascope, a change was also made in this component and improved images were obtained. A cylindrical mirror of short focal length was substituted for the refractive cylindrical lens which acted as the anamorphascope.

The improved four foot acousto-optical imaging system is shown in Figure 24. Photographs of the optical components appear in Figure 25. Figure 26 shows object transducers used to make the resolution measurements. Optics forming cell illumination light are the same as for the previous configuration except for the large 25.4 cm cylindrical lens (96.5 cm focal length) which was positioned 3.8 cm in front of the entrance window. The anamorphic image formed near the line of focus is magnified by a cylindrical mirror 9.6 cm from the exit window. This

* Defined on page 47.

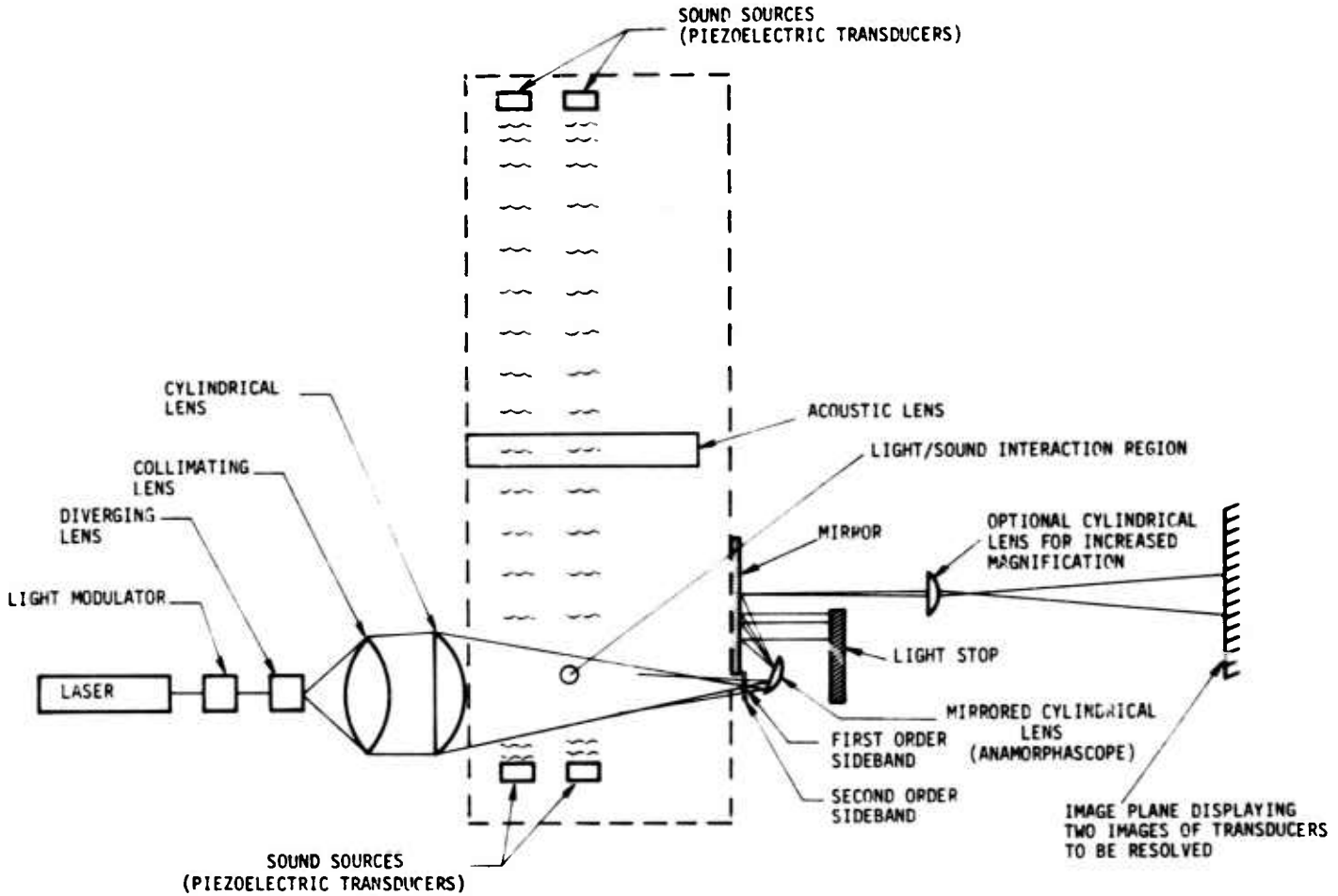

Figure 24: Second four-foot interaction cell acousto-optical imaging system.

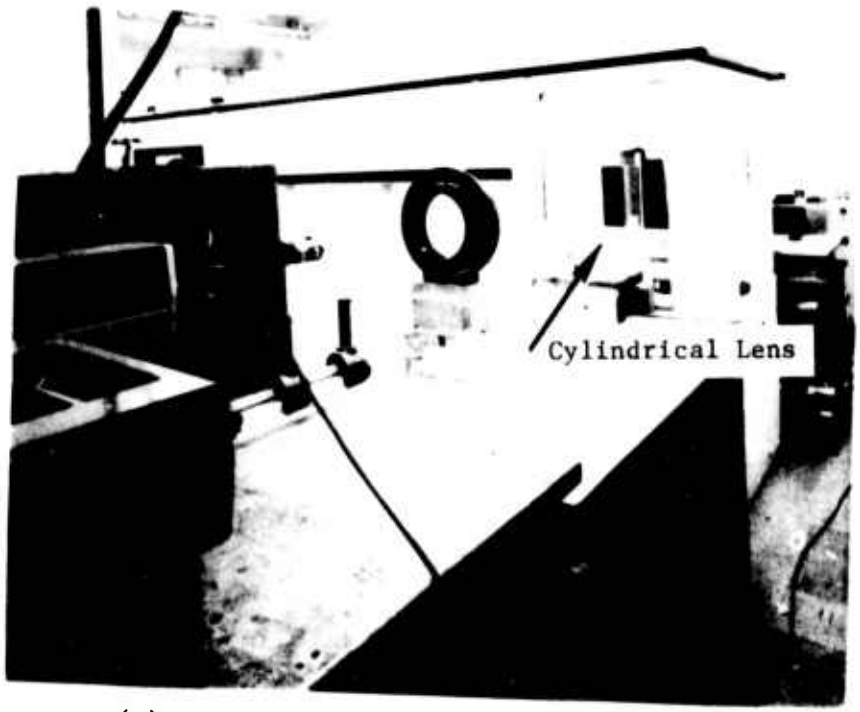

(a) Light wedge forming optics including interaction cell entrance window.

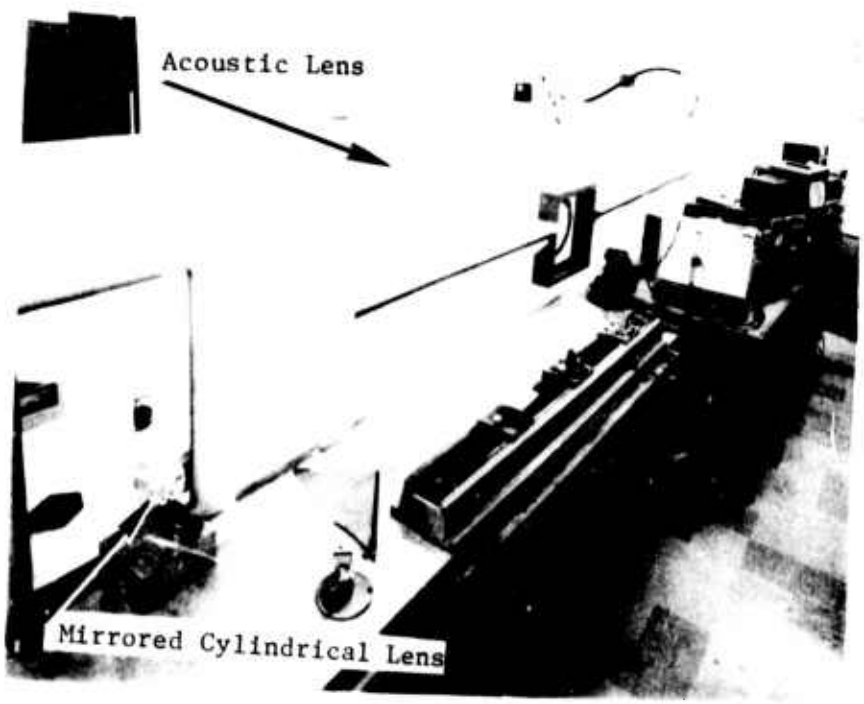

(b) Imaging optics including interaction cell exit window.

Figure 25: Optics of the improved four foot acousto-optical imaging system.

Figure 26: Object transducers used for resolution measurements in front of acoustic lens.

cylindrical mirror was made by forming a mirrored surface on the curved side of a plano-convex cylindrical lens with a focal length of 22 mm. A small mirror 8.3 cm away is used to change the direction of the image while another mirror 63.5 cm away is used to direct the image onto the image plane at a distance of 544.4 cm.

Resolution measurements were made in a similar manner to that used with the previous experimental system. After the minimum distance for clear separation was measured, the object transducers were moved closer together until the images were separated by the Rayleigh criteria. The off-axis arrangement of object transducers was not used for measurements with this acousto-optical imaging system. Measurements were taken for a frequency range from 830 KHz to 130 KHz with transducers next to the light column. Representative photographs of the images with objects 15 feet are shown in Figure 27. Figures 27a and 27b contain transducer images at 500 KHz for images separated clearly and for images separated by the Rayleigh criterion respectively. Transducer separation distances to produce images like those in Figure 27 are given in Table II.

The only system changes between the second experimental configuration just reported and the third presented here was the movement of the large (25.4 cm) cylindrical lens into the tank. Due to the increased index of refraction of water with respect to air, the effective focal length of the lens is increased. This resulted in a smaller light wedge angle and a longer light wedge as shown in Figure 28. Resolution measurements were made at frequencies in the range from 1.18 MHz to 130 KHz with the transducers next to illumination light and at the maximum possible distance, 15 feet.

Photographs of images using 50 KHz and 130 KHz sound with objects at 15 feet in the third experimental configuration are shown in Figure 29. Figures 29a and 29b are clearly separated images at frequencies of 130 KHz and 50 KHz, respectively. Poor quality of the images is due to the small number of resolution cells available for

(a) Images of two transducers at 500 KHz of separation for clearly separated images.

(b) Rayleigh criterion images at 500 KHz.

(c) Images of two transducers at 130 KHz of separation for clearly separated images.

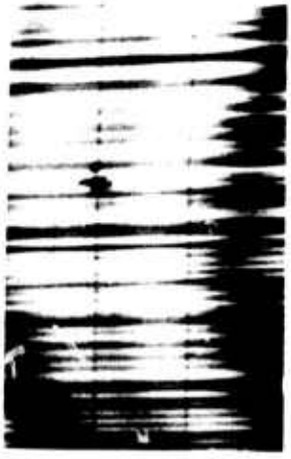

(d) Rayleigh criterion images at 130 KHz.

Figure 27: Images formed with the object transducers at a distance of 15 feet using the improved four-foot experimental configuration.

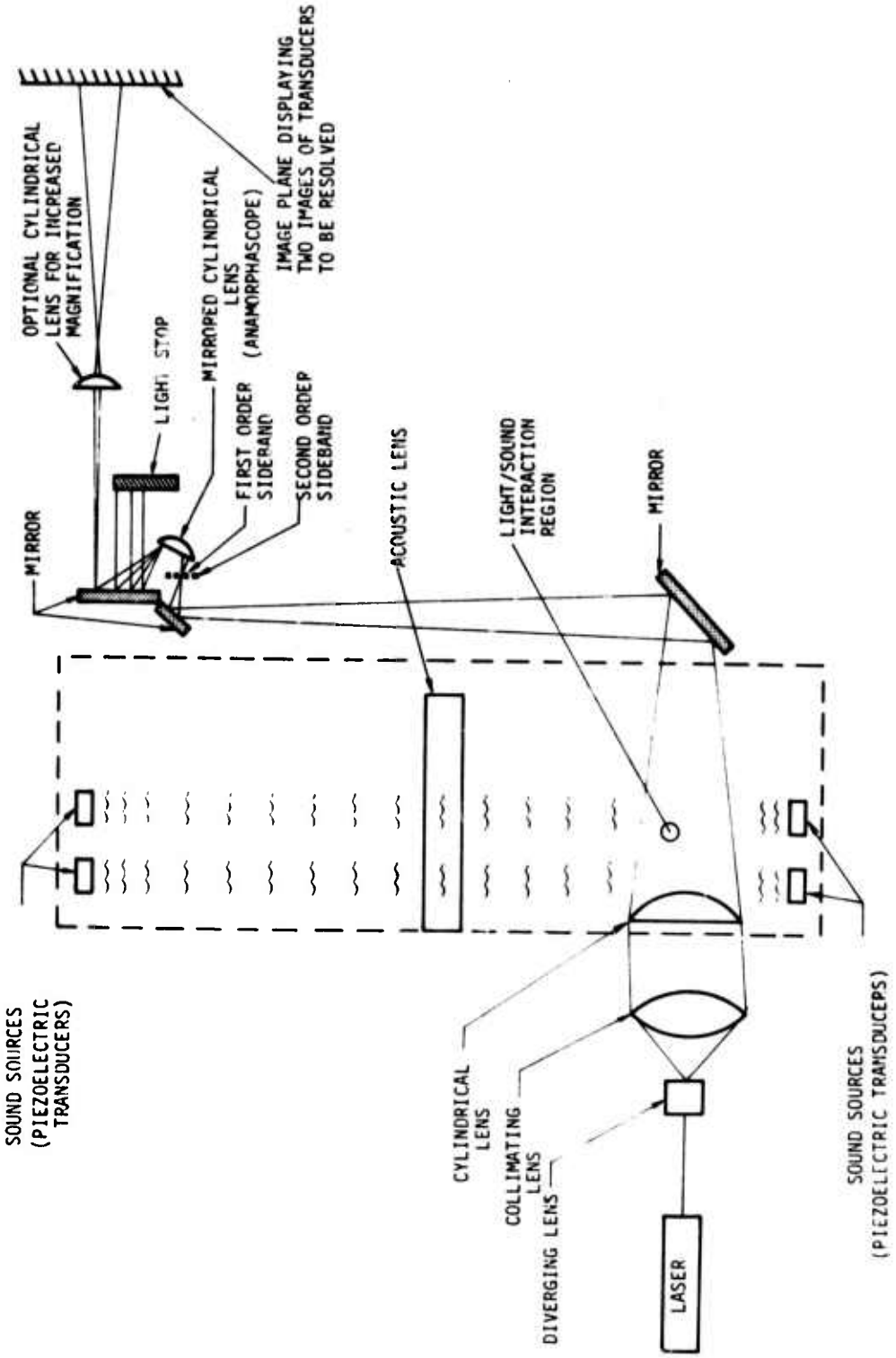

Figure 28: Third four-foot interaction cell acousto-optical imaging system.

Table II: Resolution measurements for the second four foot (1.22 meter) acousto-optical imaging system configuration.

TRANSDUCERS NEXT TO THE LIGHT COLUMN		
Frequency	Measured Resolution Transducers On Axis	$\Lambda/2 \sin \alpha$
830 KHz	5.1 cm	.7 cm
500 KHz	12.7 cm	1.1 cm
160 KHz	26.6 cm	3.5 cm
130 KHz	48.3 cm	4.3 cm

TRANSDUCERS AT A DISTANCE OF 5 METERS				
Frequency	Separation of Transducers on Axis for Clearly Separated Images	Measured Resolution Transducers On Axis (Rayleigh Criterion)	$\Lambda/2 \sin \alpha$	Λ R/D
1.8 MHz	2.5 cm		.3 cm	.3 cm
1.18 MHz	7.6 cm	3.6 cm	.5 cm	.5 cm
500 KHz	21.6 cm	8.9 cm	1.1 cm	1.1 cm
160 KHz	30.4 cm	27.9 cm	3.5 cm	3.5 cm
130 KHz	38.0 cm	26.1 cm	4.3 cm	4.3 cm

(a) Images of two transducers at 130 KHz.

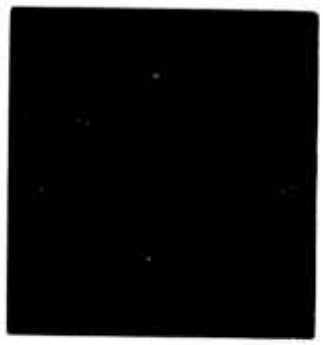

(b) Central order light and an image of one transducer at 50 KHz.

Figure 29: Images formed using cell configuration shown in Figure 28.

image formation. For example, there is room for no more than three resolution cells at 50 KHz. Resolution measurements for this system are given in Table III.

Table III: Resolution measurements for the third four-foot (1.22 meter) Bragg cell acousto-optical imaging system configuration.

Frequency	Measured Resolution Transducers on Axis	$\Lambda/2 \sin \alpha$
TRANSDUCERS NEARBY		
1.18 MHz	12.7 cm	3.9 cm
830 KHz	15.2 cm	5.4 cm
160 KHz	66.2 cm	27.1 cm
130 KHz	94.0 cm	34.0 cm
TRANSDUCERS AT A DISTANCE OF 15 FEET		
1.8 MHz	7.7 cm	2.5 cm
830 KHz	13.6 cm	5.4 cm
500 KHz	24.8 cm	9.0 cm
130 KHz	54.7 cm	34.0 cm

The quality of these images is inferior to the quality of the images produced with the second experimental configuration. Such a degradation in image quality is indicated by the expression for resolution

$$\delta = \Lambda/2 \sin \alpha$$

where δ = resolution

Λ = the wavelength of sound involved

2α = the wedge angle of the light column of the Bragg cell

This expression shows that the decrease in the wedge angle increased the resolution cell size. The importance of the third experimental configuration is that the longer light wedge resulted in increased image separation from the wedge focal line as expected from theory. A transducer image at 50 KHz was clearly separated for the first time. The separations of sideband images from the central order light for frequencies of 160, 130 and 50 KHz are compared in Table IV below. The inclined, rather than vertical, nature of the images shown are a result of a slight tilt of the anamorphascope. More care would have resulted in elongated patches of light which are vertically oriented.

Table IV: Separation measurements

Frequency	4-Foot Wedge	16-Foot Wedge
160 KHz	5.1 cm	15.2 cm
130 KHz	1.3 cm	8.9 cm
50 KHz	No Separation	1.3 cm

A selected comparison of measurements with the object next to the light column as a function of the light wedge angle is shown in Table V below.

Table V: Resolution comparison

Frequency	WEDGE HALF ANGLE		
	α_1 = .967°	α_2 = 7.68°	α_3 = .967°
830 KHz	15.3 cm	5.1 cm	15.2 cm
160 KHz	57.2 cm	26.6 cm	66.2 cm

NOTE: α_1, α_2 and α_3 were half angles in the experimental configurations shown in Figures 19, 24 and 28, respectively.

These results indicate that better resolution is obtained for larger wedge angles (as predicted by theory). This agrees with the expression, $\delta = \Lambda/2 \sin \alpha$ that an increase in light wedge angle increases

resolution. For the same incident light geometry the light wedge angle decreases as the wedge length increases. These are important considerations for optimizing an acousto-optical imaging system.

3.4 Image Formation Experiments

The four-foot acousto-optical imaging system, shown in Figure 30, was used to obtain images by sound reflection from objects at a distance of 15 feet (4.6 m) from the light-sound interaction region. These images have been formed at a variety of frequencies from 1.8 MHz to 280 KHz. Figure 31a shows an object used for reflection imaging. The image of this object is shown in Figure 31b. An image of the same object formed on a TV monitor appears in Figure 31c. Using the brightness control on a television monitor, excess scattered light can be reduced and contrast increased to obtain the image improvements which are quite apparent.

The remaining images presented here were formed by inclusion of the optional cylindrical lens shown in Figure 30 to increase magnification in the horizontal direction.

When viewing image photographs, the reader should be aware of the difference attributed entirely to exposure time. Figures 32b and 32c are different photographic exposures of the object shown in Figure 32a. Figure 32d is an image of that object as seen on the television monitor.

Using the same object as shown in Figure 32a, the acoustic frequency was varied from 1.8 MHz to 500 KHz resulting in both the directly viewed and TV monitored images of Figure 33. Since a resolution cell size increases as the frequency decreases, the images degenerate with decreasing frequency. A larger object, Figure 34a, was used to form images at 500 KHz and 280 KHz. It is clearly demonstrated by comparing the images of both objects at 500 KHz that any object larger than the resolution cell size can be imaged while an object smaller than the resolution cell size cannot. The sound field of the object illumination transducer and the geometry of the tank prevented further reflection imaging of larger objects at lower frequencies.

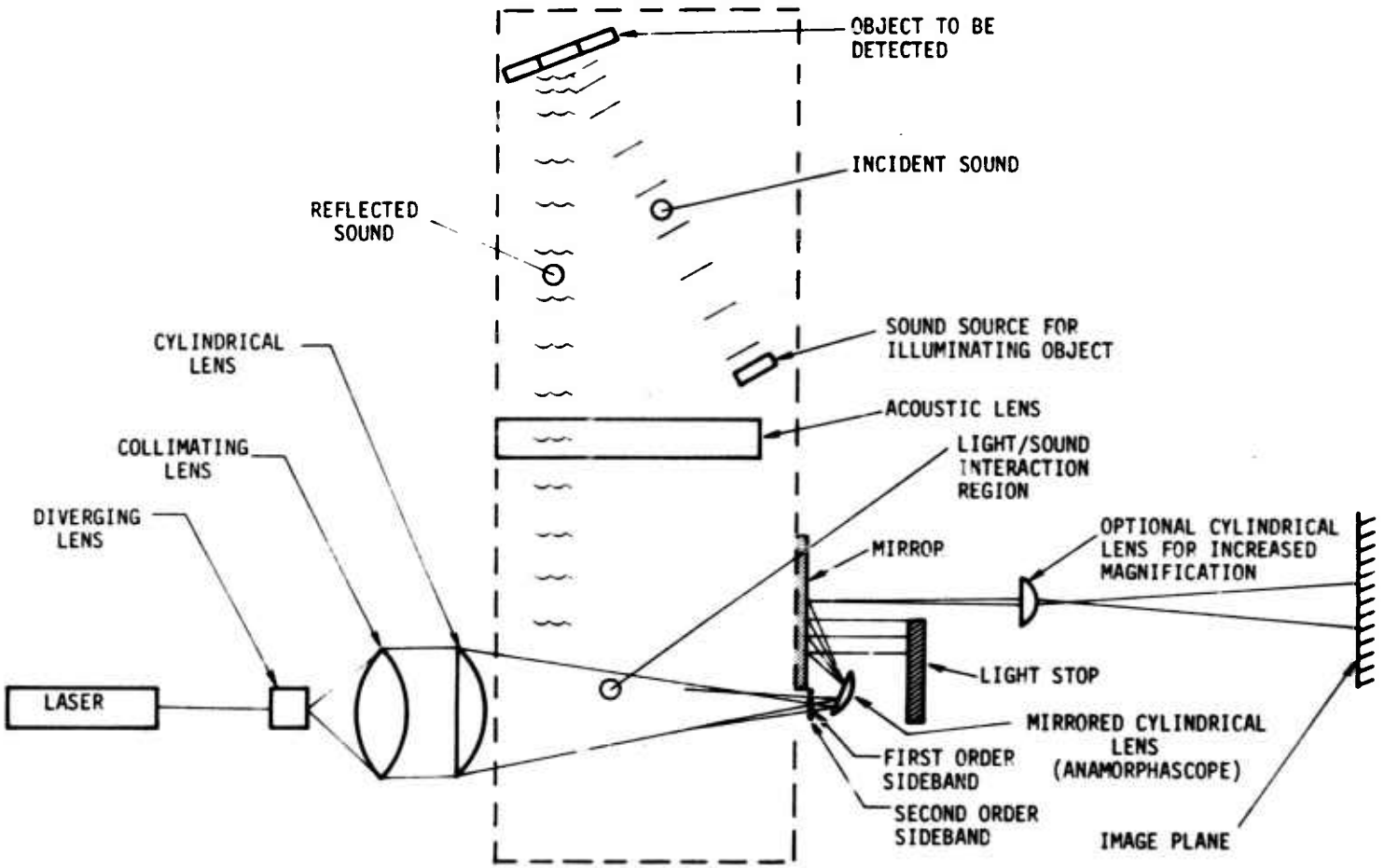

Figure 30: Four-foot interaction cell used for reflection imaging.

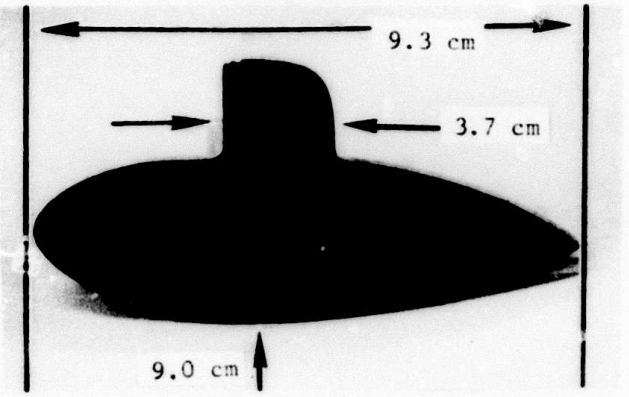

(a) Objects used for reflection imaging.

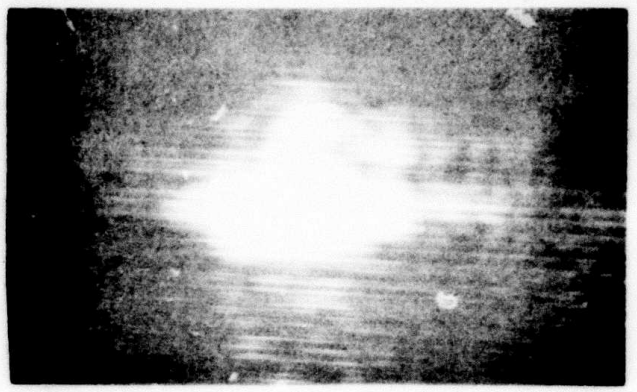

(b) Direct image of above object at 1.8 MHz.

(c) TV image of above object at 1.8 MHz.

Figure 31: Reflection images at 1.8 MHz at a distance of 15 feet.

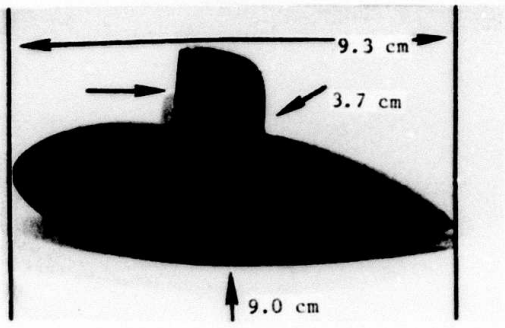

(a) Object used for reflection imaging

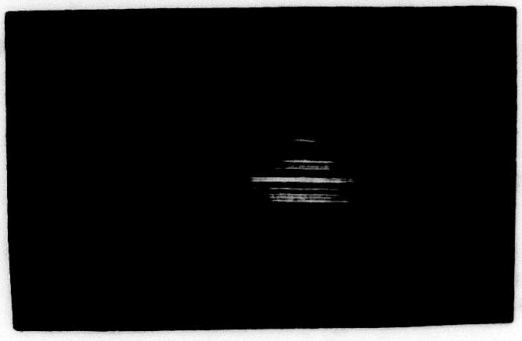

(b) Shorter photographic exposure of direct image at 1.8 MHz

(c) Long photographic exposure of direct image at 1.8 MHz

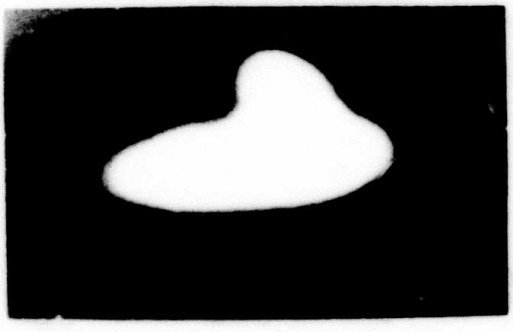

(d) TV image of above object at 1.8 MHz

Figure 32: Reflection images at 1.8 MHz at a distance of 15 feet.

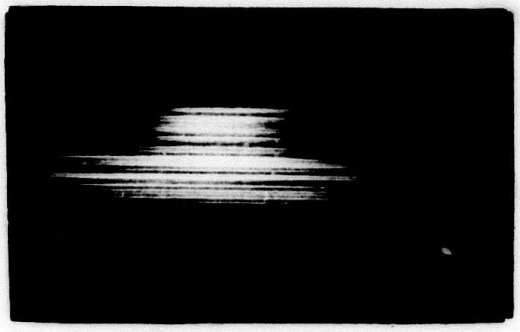

(a) Direct image at 1.25 MHz

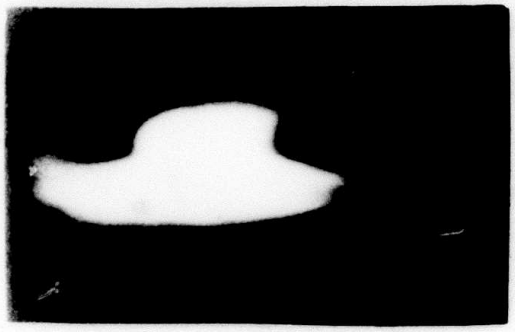

(b) TV image at 1.25 MHz

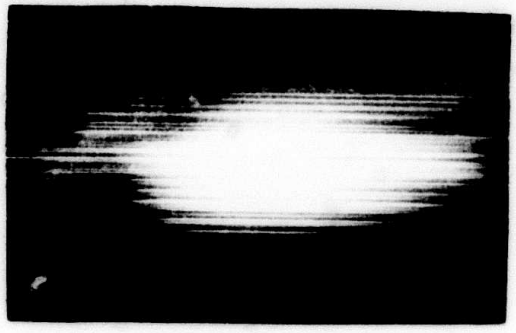

(c) Direct image at 980 KHz

(d) TV image at 980 KHz

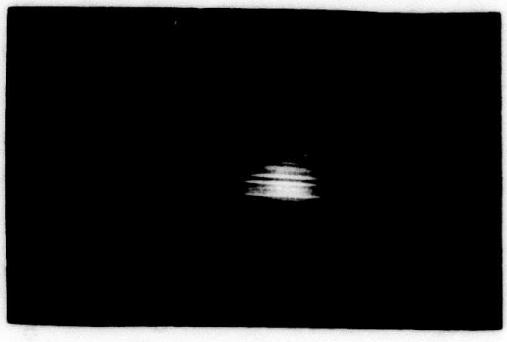

(e) Direct image at 500 KHz

(f) TV image at 500 KHz

Figure 33: Reflection images of the object of Figure 32a at a distance of 15 feet.

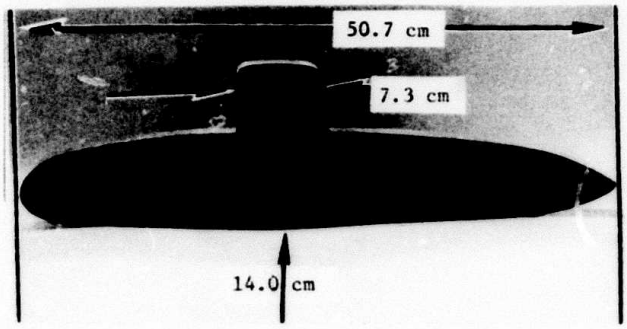

(a) Object used for 500 KHz and 280 KHz reflection imaging

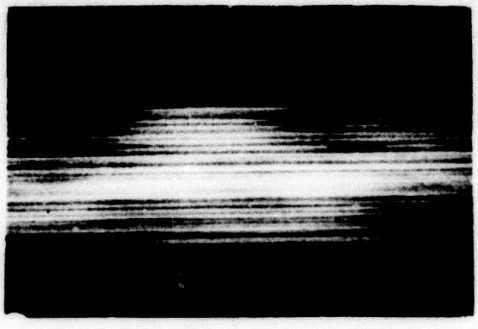

(b) Direct image of above object at 500 KHz

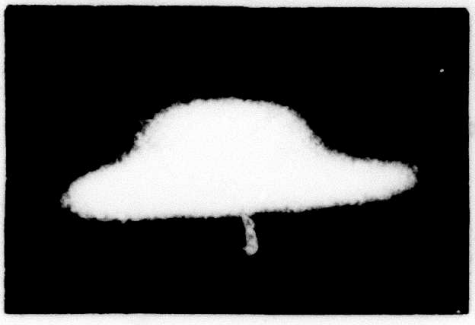

(c) TV image of above object at 500 KHz

(d) Direct image of above object at 280 KHz

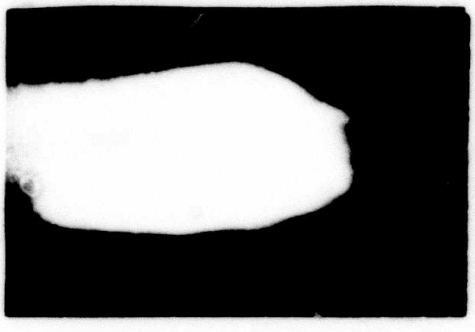

(e) TV image of above object at 280 KHz

Figure 34: Reflection images at 500 KHz and 280 KHz at a distance of 15 feet.

3.5 Field of View Experiments

The current TRW Acousto-Optical Imaging System has been employed in an experiment to measure field of view. The only variation from the standard experimental configuration was the insertion of a six-inch aperture between the light wedge and the object transducer, Figure 35. The one-inch object transducer was then moved parallel to the light wedge and rotated to produce maximum image intensity at each experimental point. At a distance of six feet from the aperture and at a frequency of 3.5 MHz, the intensity was measured as a function of cross-range distance. A plot of relative image intensity versus cross-range distance is shown in Figure 36. From this figure it appears that the field-of-view for image viewing with the naked eye is limited to the size of the aperture (as predicted by theory).

3.6 Discrimination of Wave Arrival Direction

A spectrum analysis of light in image sidebands was performed to observe the expected discrimination of wave arrival direction. This was observed by comparing the relative intensities of the signals at the sum and difference frequency for two configurations of the object transducers as shown in Figure 37. This rejection phenomenon indicates that the acousto-optical imaging system is sensitive to the sound wave propagation direction. The directional rejection measurements are given in Table VI below.

Table VI: Directional rejection levels

Level at Sum Frequency	Level at Difference Frequency	Rejection Level
Transducers on Opposite Sides of Light		
-49 db	-60 db	11 db
Transducers on Same Side of Light		
-91 db	-56 db	35 db

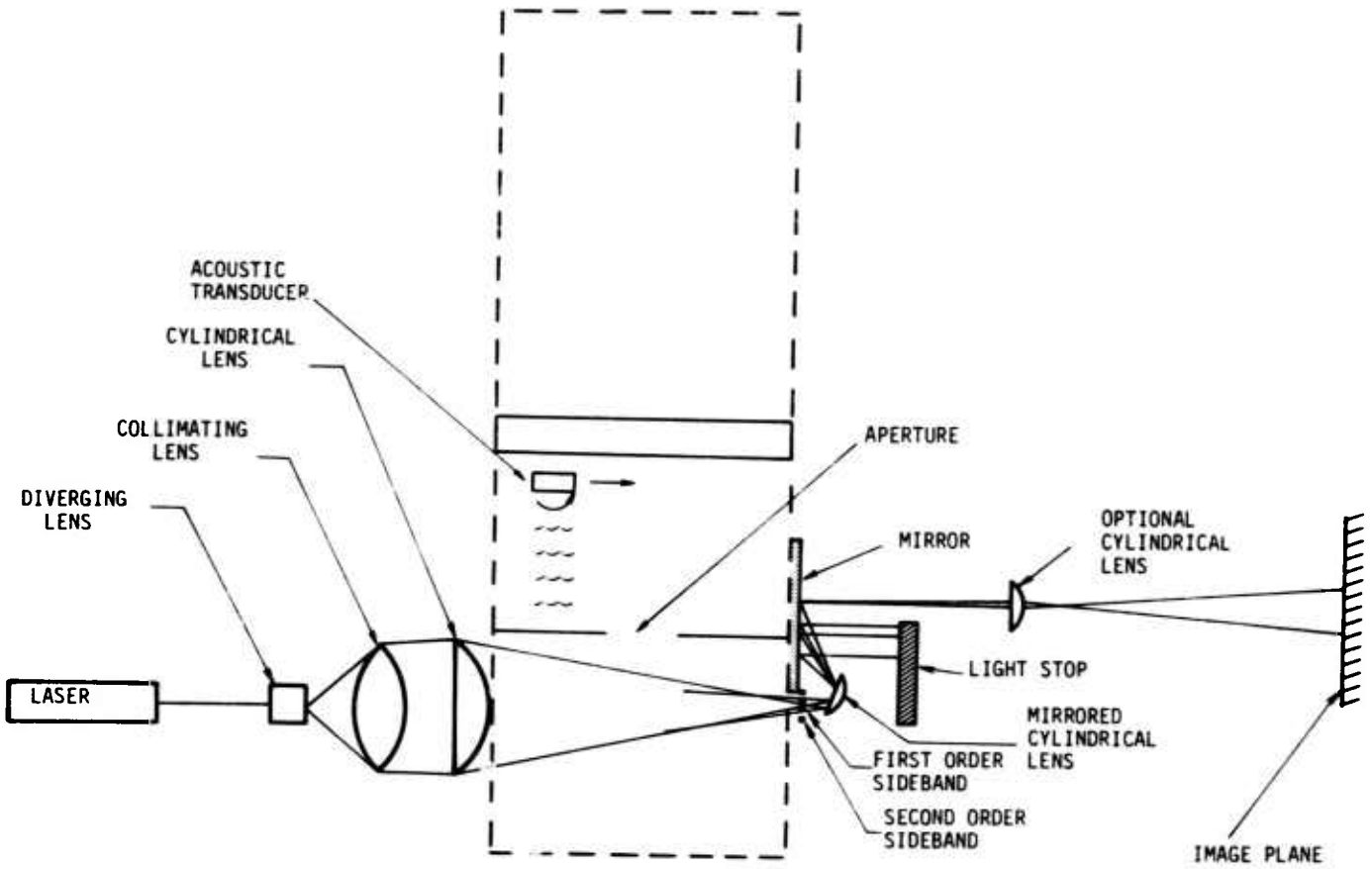

Figure 35: Four-foot interaction cell used for field of view measurement.

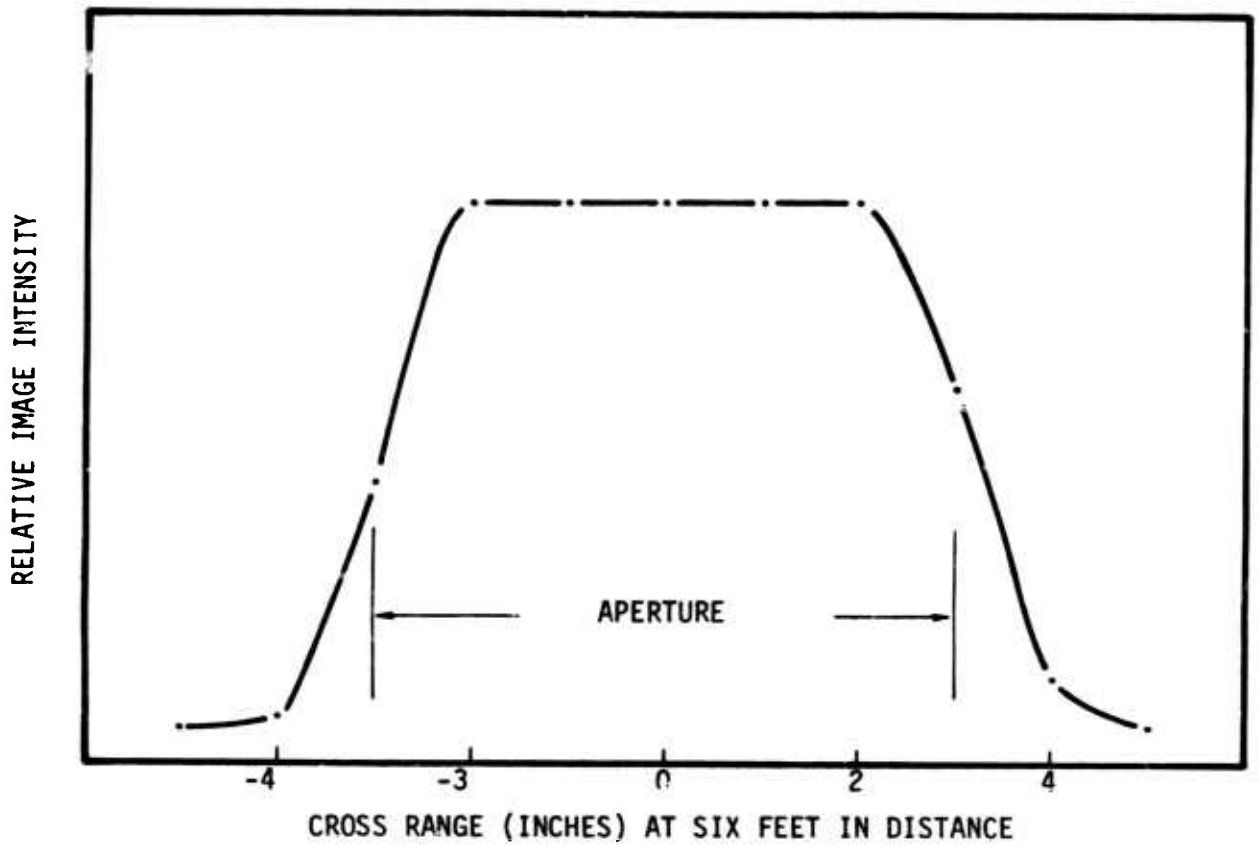

Figure 36: Relative image intensity as a function of cross-range distance.

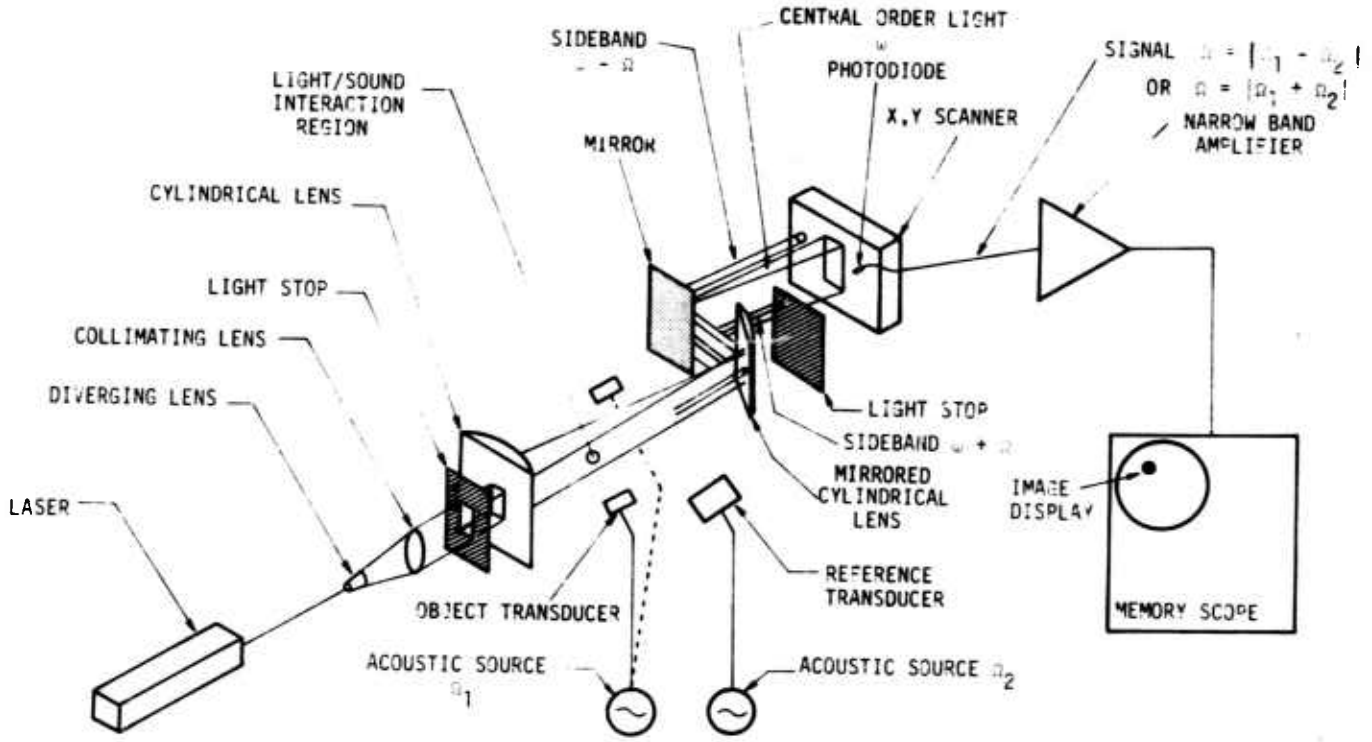

Figure 37: Experimental configuration to determine the discrimination of wave arrival direction.

The discrepancy between the rejection levels can be attributed to asymmetry of the sum and difference frequency configurations and geometry of the tank. The object transducer was aimed towards the near end of the tank in the sum frequency configuration. Here sound reflections can increase the difference frequency levels. However, these reflections would not be present in the difference frequency configuration. Therefore, these results indicate that an acousto-optical imaging system could have a directional noise rejection as high as 35 db.

4.0 PROJECTED PERFORMANCE OF A HIGH RESOLUTION IMAGING SONAR

4.1 Range Calculations

Predicted ranges for the TRW Acousto-Optical Imaging System have been calculated as a function of temperature, salinity, depth, frequency and particulate concentration. This has been accomplished using a computer program (Appendix B) which solves the basic two way transmission sonar equations (Ref. 13). Reverberations were neglected since inclusion would make it quite difficult to compare this system with alternatives. Additionally, imaging implies that sound arriving from different directions due to reflections at the same range will show up in different parts of the image and therefore, will not degrade operating range.

$$SL - 2TL + TS = EL \tag{23}$$

where SL = source level

$TL = 20 \log R + \alpha R \times 10^{-3} + \alpha_p R$

R = range

α = logarithmic absorption coefficient

α_p = logarithmic absorption coefficient due to particle concentration

TS = target strength = 0 db

EL = minimum detectable echo

The source level was assumed to be on the order of the cavitation level at the surface (117 db) with the transmitting directivity index of an ideal circular piston transducer of one meter diameter. An ideal circular piston transducer is equivalent to a parallel beam array with a one meter aperture. The logarithmic absorption coefficient, α, was calculated using the equation of Schulkin and Marsh (Ref. 13)

$$\alpha = ASf_T f^2/(f_T^2 + f^2) + Bf^2/f_T$$

$$f_T = 21.9 \times 10^6 - 1520/(T + 273) \tag{24}$$

where A,B = constants

S = salinity in parts per thousand

f = acoustic frequency in kilohertz

T = temperature in degrees centigrade

α_p was calculated using the Eq. (14)

$$2\alpha_p = C\ ka^3/3 + k(\sigma - 1)^2\ S/\ S^2 + (\sigma + \tau)^2 \qquad (25)$$

where C = total volume concentration of the particles

k = wave number of the acoustic signal

a = effective particle radius = 4 microns

τ = particle density/water density = 2.65

$S = 9/4\ a\ (1 + 1/\beta a)$

$\tau = 1/2 + 9/4\beta a$

$\beta = (\omega/2\mu)^{1/2}$

ω = angular frequency

μ = kinematic fluid viscosity

The target strength was assumed to be zero. The minimum detectable echo was the value experimentally determined using the present laboratory TRW Acousto-Optical Imaging System. After substitution of Eqs. (24) and (25) into the sonar equation for two way transmission, the equation was solved for range using the bi-section method of iteration.

Figure 38 is a plot of range vs. frequency with depth as a parameter. This figure shows that range has a very weak dependence on depth for the operating depths and frequencies which would be employed by the TRW Acousto-Optical Imaging System.

The effect of salinity on system performance was evaluated by using the reference computer program. The results appear in Figure 39, which shows a maximum range variation of about 25 percent over

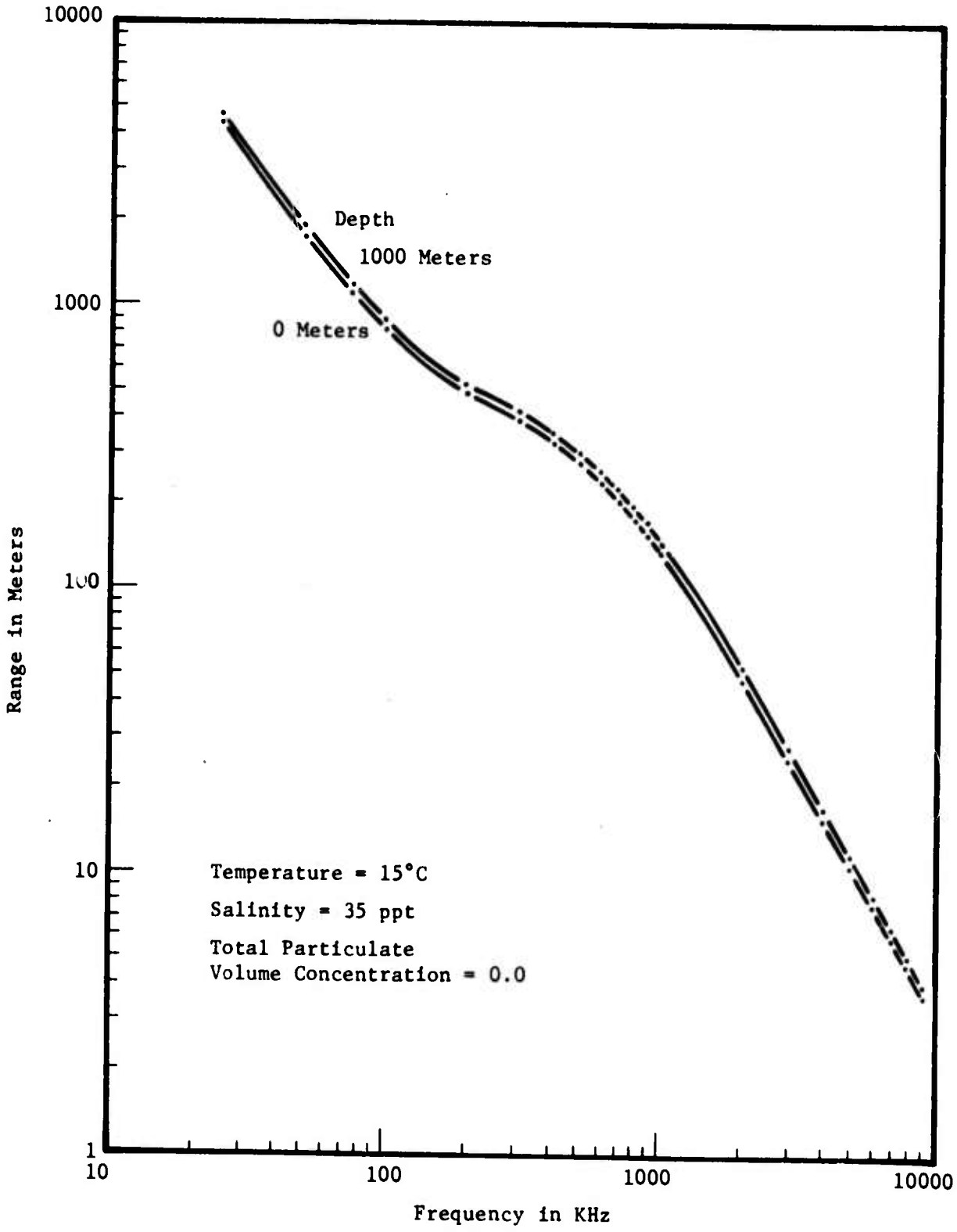

Figure 38: Dependence of range as a function of frequency with depth as a parameter.

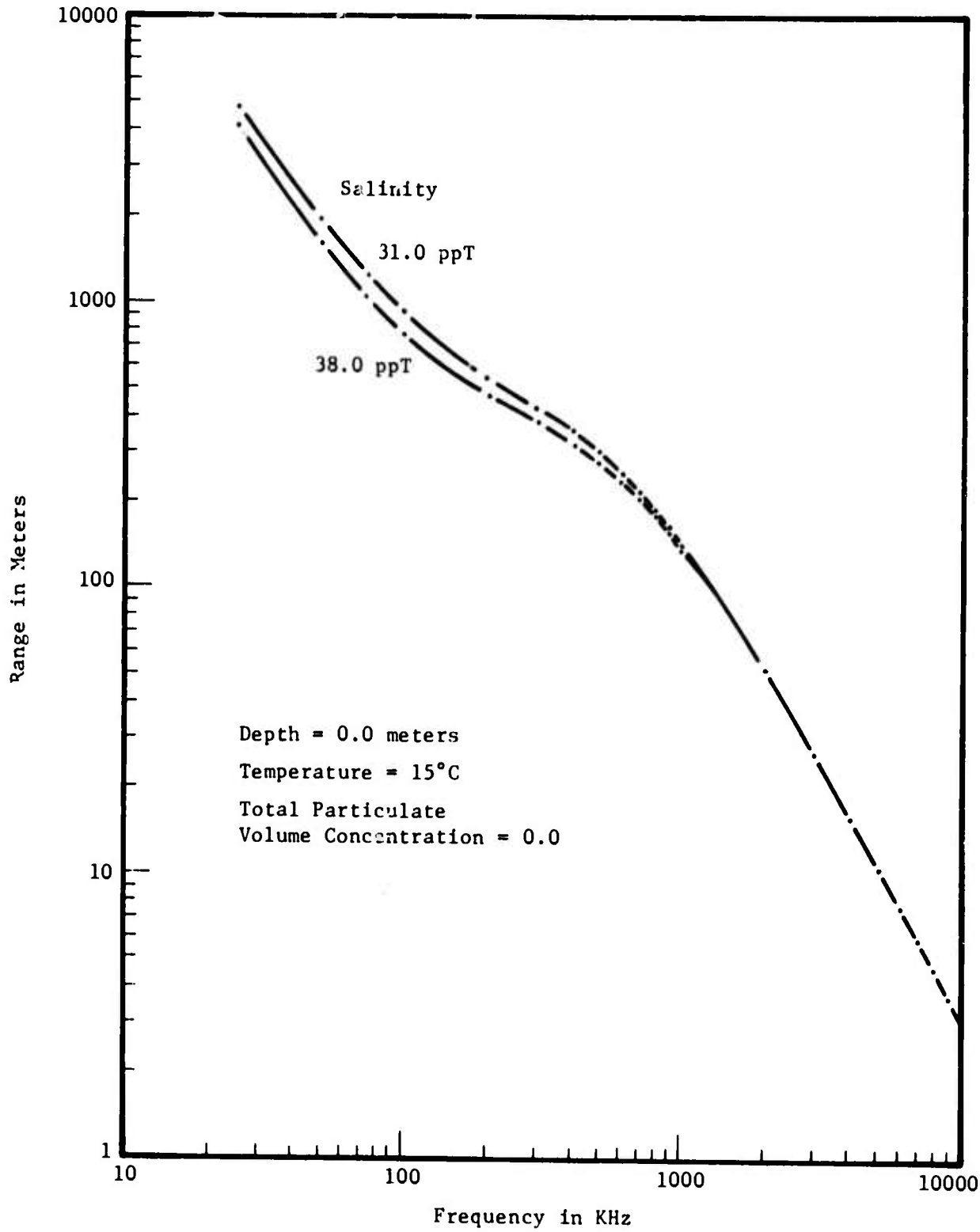

Figure 39: Dependence of range on frequency with salinity as a parameter.

extreme salinity changes. Figures 40 and 41 show the effects of volume particle concentration on range. The first figure displays a curve family for range vs. particulate volume concentration with frequency as a parameter. The second figure is the family of curves for range vs. frequency with particulate volume concentration as a parameter. Both of these curve families reveal an extreme reduction in range as particulate concentration increases. The plots of range as a function of temperature with frequency as a parameter and range as a function of frequency with temperature as a parameter are shown in Figures 42 and 43, respectively. A 10 degree centigrade change in temperature can result in a maximum variation of about 30 percent in range. All of the above plots reveal the extreme effect of frequency on range for any acoustic system. Range is most strongly dependent on the variables of frequency and particulate concentration. However, any acousto-optical imaging system would have to be designed with regard for the application and environmental effects of all these parameters.

4.2 Operational Configuration

Figure 44 shows an external view of a workable configuration which uses the TRW Acousto-Optical Imaging approach. This figure shows what is called the sonar head for receiving sound reflected from a distant object. This receiving head has the maximum dimension of one meter in each direction as illustrated. The construction of the head is quite simple. It simply consists of a volume of clean water which is kept clean by a radome that isolates external seawater from clean water contained within the head. This head is backed up by an acoustic reflector which forms the field of view in the vertical direction. For simplification of the discussion consider that the vertical direction is normal to the axis of symmetry for the acoustic reflector and cell illumination light. Cell illumination light is shown as a wedge of light. It is a horizontal convergent section of light formed by the large cylindrical lens at the right side of the

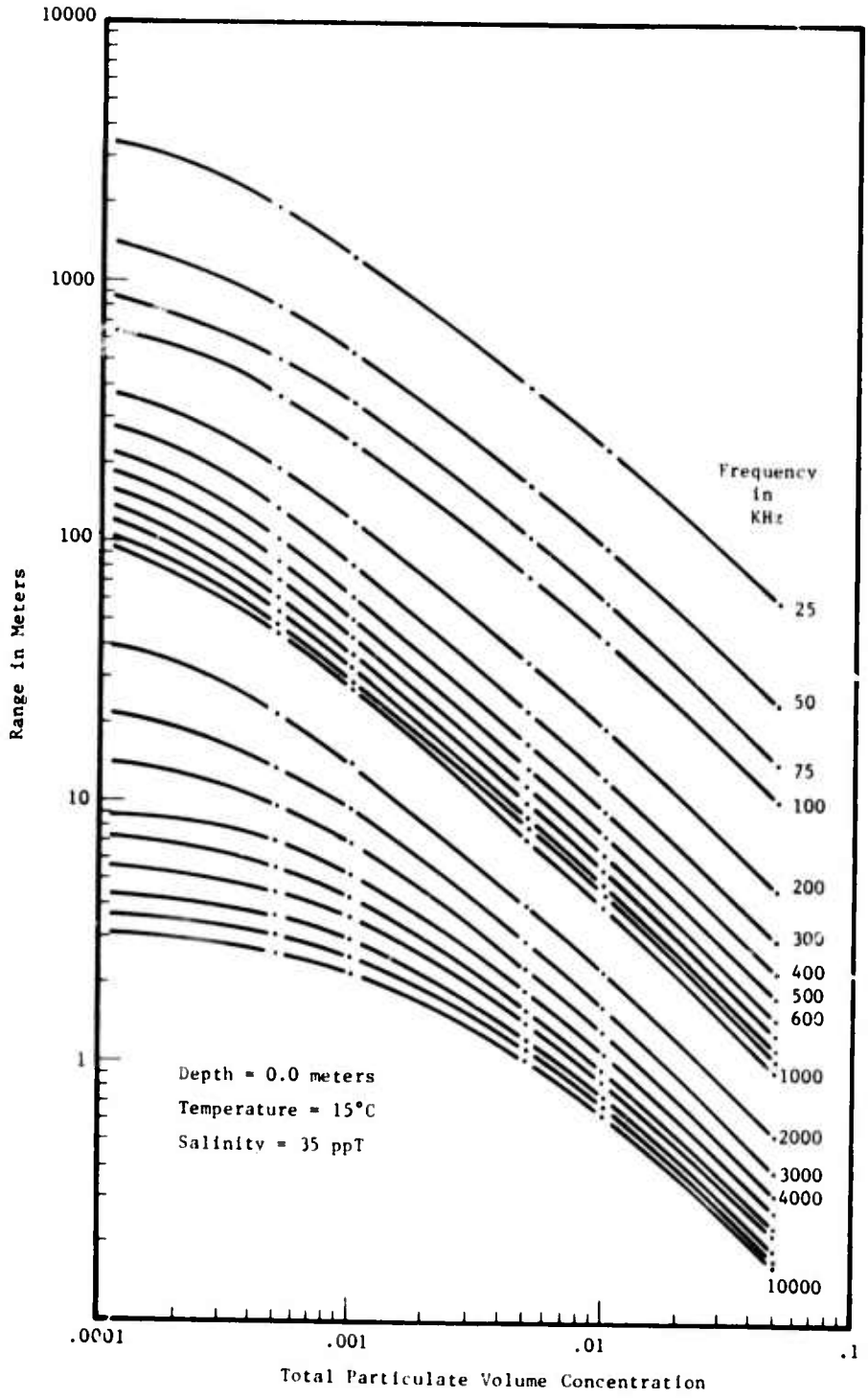

Figure 40: Range capability under dirty water conditions.

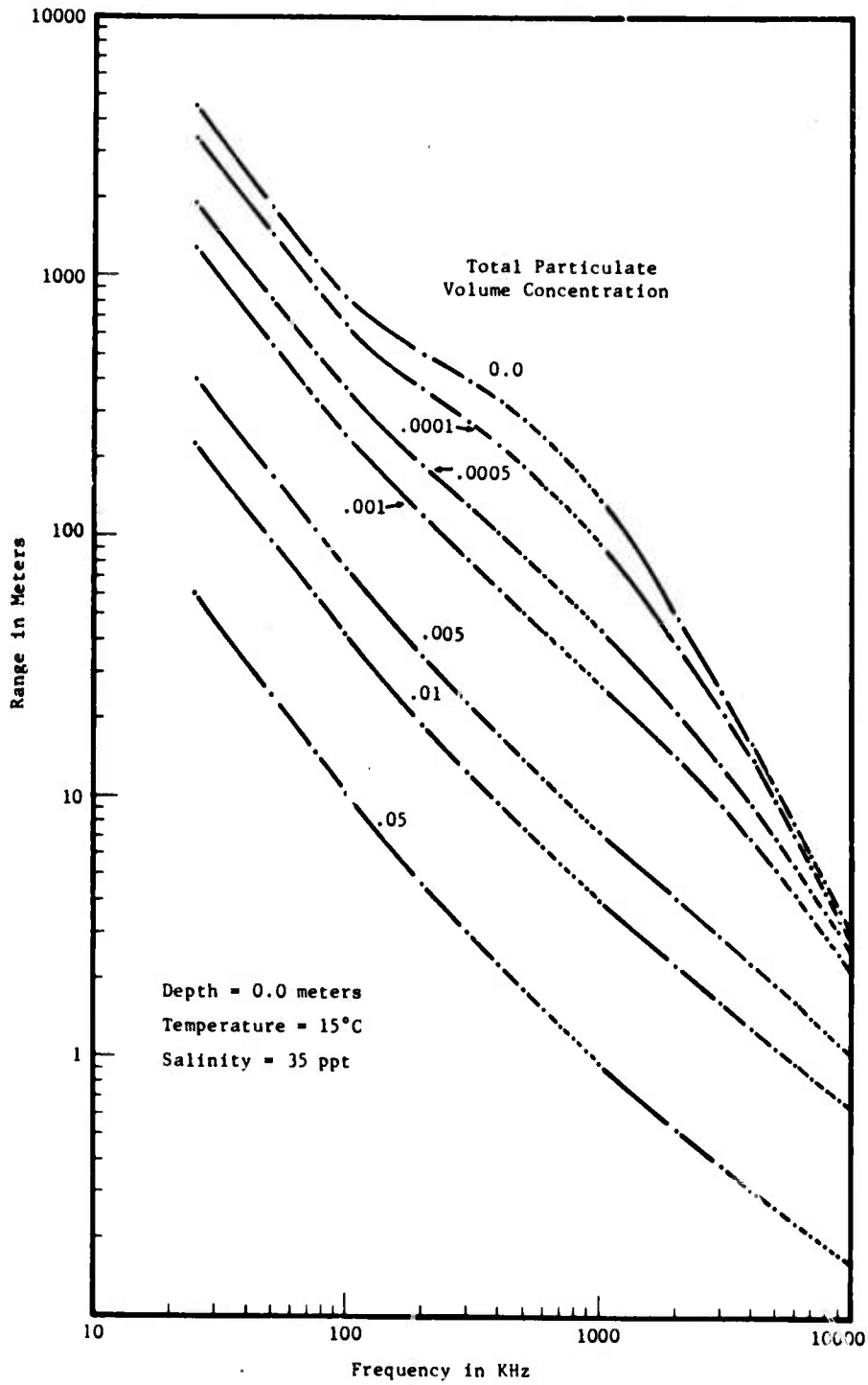

Figure 41: Dependence of range on frequency with particulate volume concentration as a parameter.

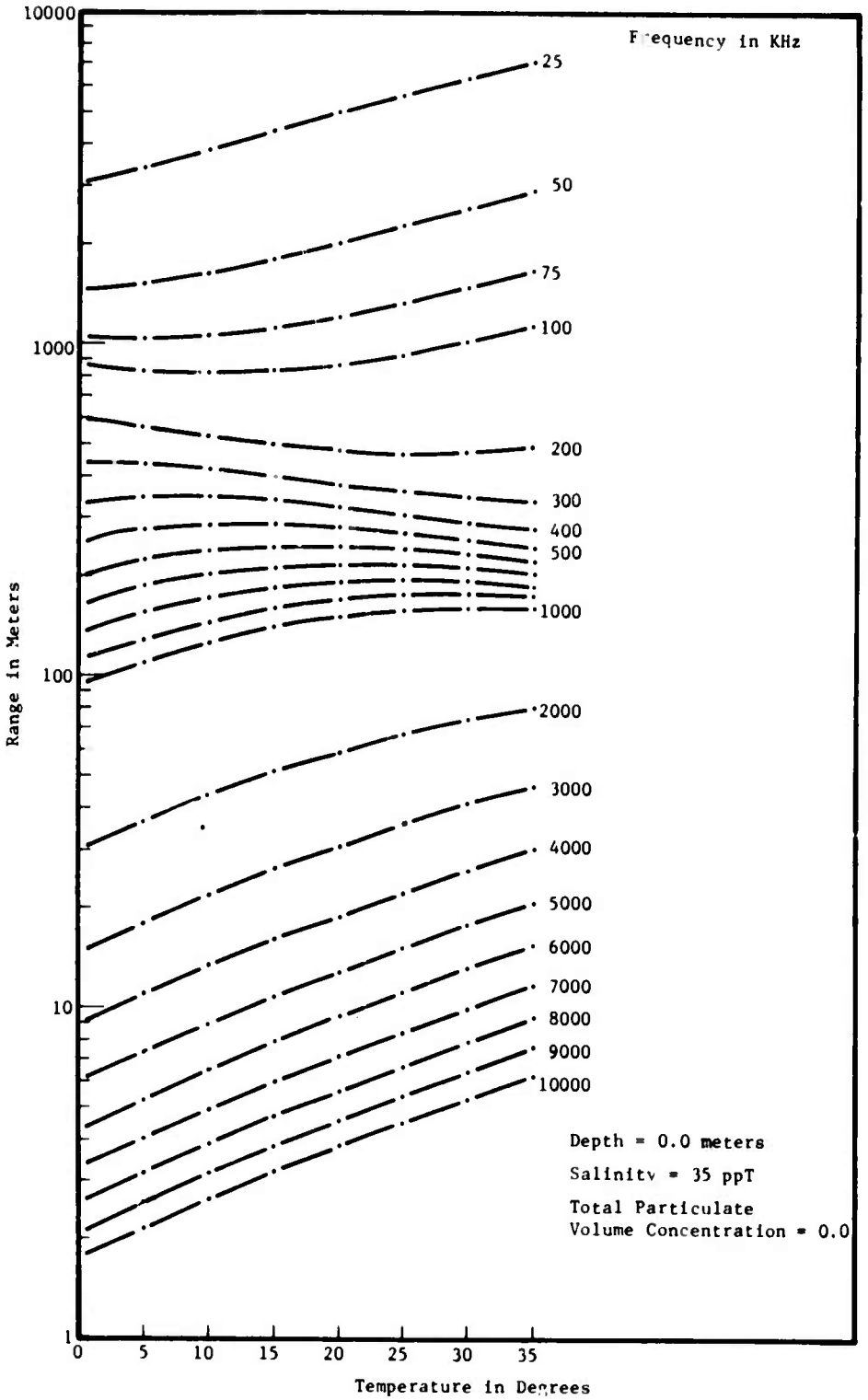

Figure 42: Dependence of range as a function of temperature with frequency as a parameter.

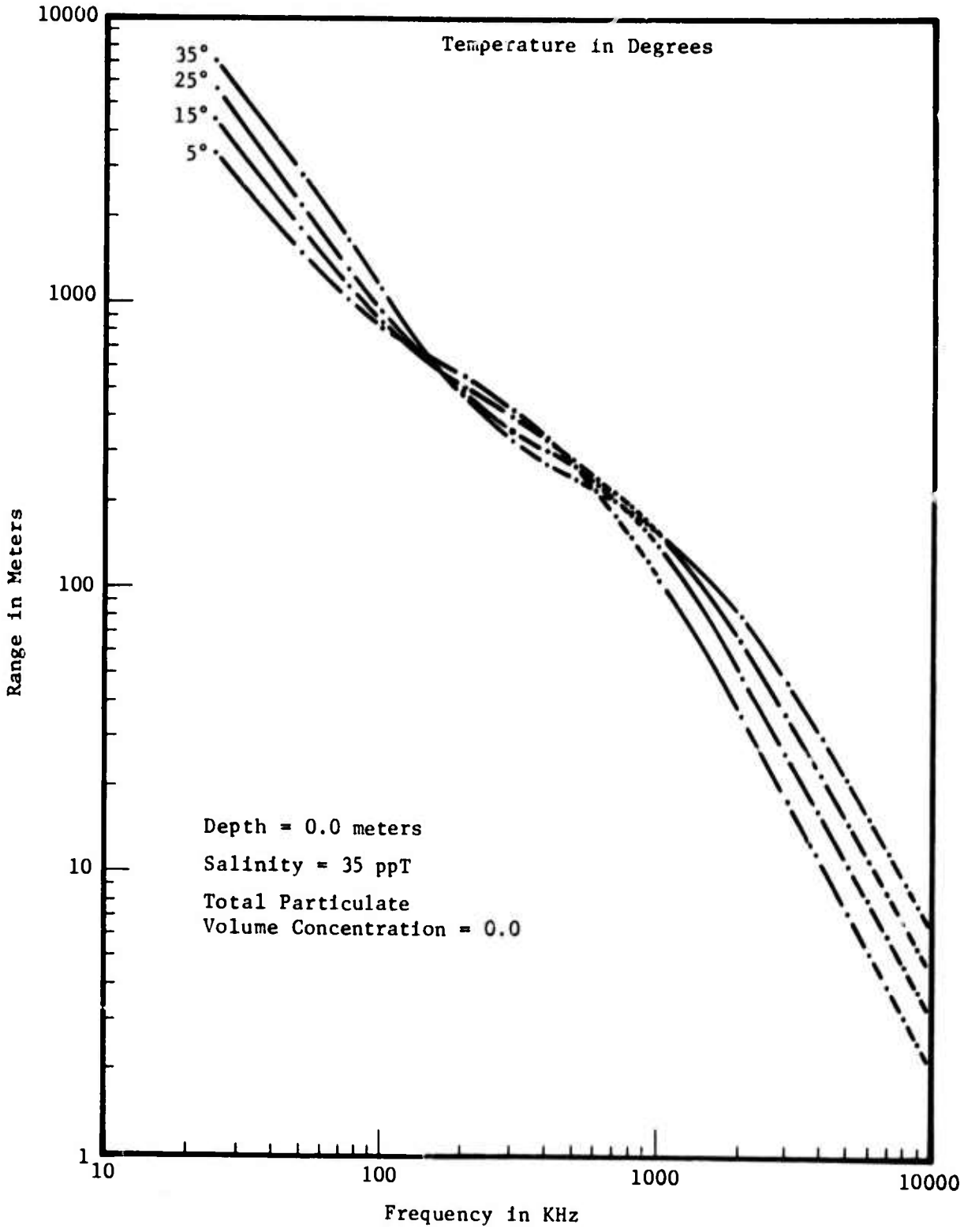

Figure 43: Dependence of range as a function of frequency with temperature as a parameter.

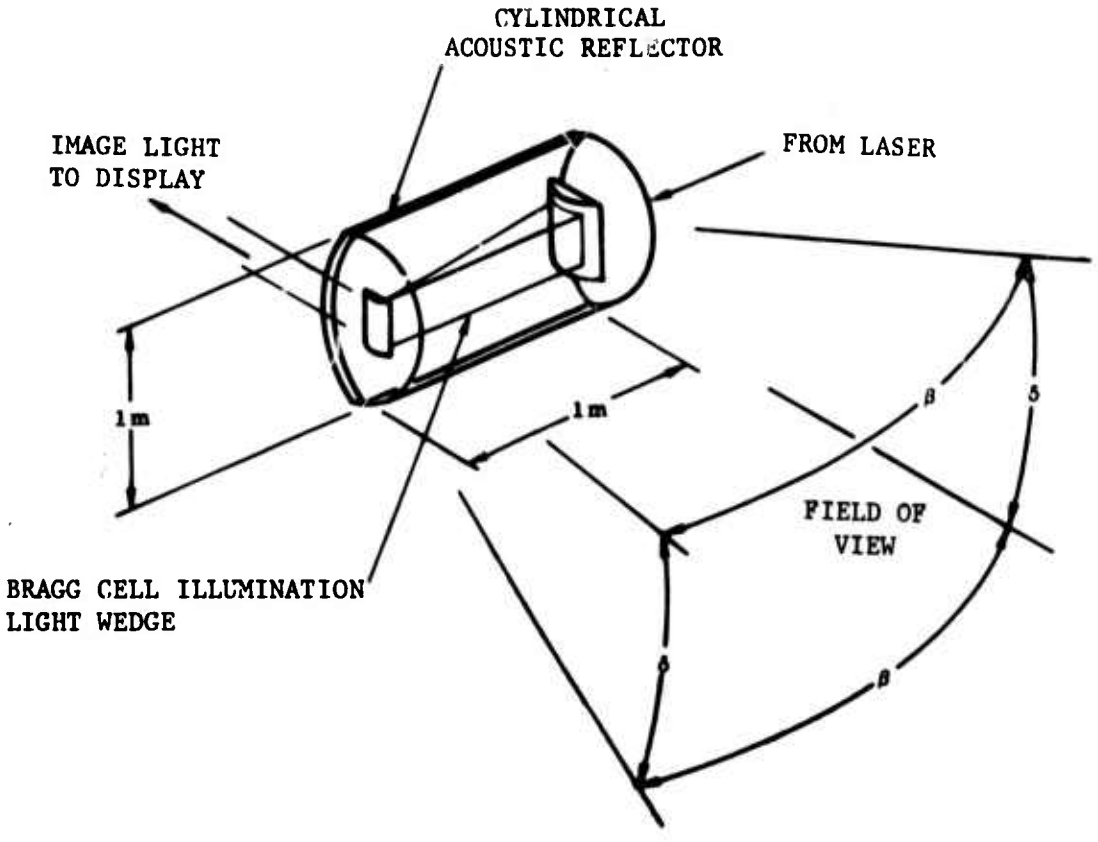

Figure 44: External view of TRW acousto-optical imaging sonar.

sonar head. Only clean water and the illuminating light wedge are located within the radome. A second cylindrical lens is located on the left side of this sonar head as shown in Figure 44. The second cylindrical lens is a lens of short focal length which actually would be a combined lens-mirror arrangement. This lens-mirror arrangement is designed to magnify while causing light to bend through a right angle so that the image will be formed behind the sonar head and internal to the vehicle which supports the sonar head. The imaging array of photosensors is placed to receive light which has been reflected from this lens-mirror arrangement. This is in the general direction labeled "to display" in Figure 44.

Estimates of the range and resolution of a system with 1 meter aperture are given in Tables VII and VIII. At large ranges, resolution will approach the diffraction limit set by the acoustic aperture. This occurs because a large spot size is predicted by the small numerical aperture available for intercept of acoustic waves when the object is at a great distance. Imperfections in the optics are then masked by the gross nature of the image. For estimating purposes, dirty water was assumed to consist of 0.1% by volume of 4. μm particles. Range capability is based on use of a focused sound projector operating on the order of the cavitation limit (.33 watts/cm^2) at the surface and that system sensitivity is equal to the levels measured for the laboratory experimental system. The effect of target strength on range is indicated in Figure 45.

Table VII: Operating characteristics of the TRW Acousto-Optical Imaging System for dirty water.

Operating Range	Frequency of Sound	Resolution (Cross-Range)
64 meters	400 KHz	24.0 cm
100 meters	246 KHz	61.0 cm
200 meters	122 KHz	245.9 cm

NOTE: Water temperature = 15°C
Acoustic aperture = 1 meter

A similar calculation for the case with clean salt water is given in Table VIII.

Table VIII: Operating characteristics of the TRW Acousto-Optical Imaging System for clean water.

Operating Range	Frequency of Sound	Resolution (Cross-Range)
100 meters	1.28 MHz	11.7 cm
200 meters	740 KHz	40.5 cm
337 meters	400 KHz	130.0 cm

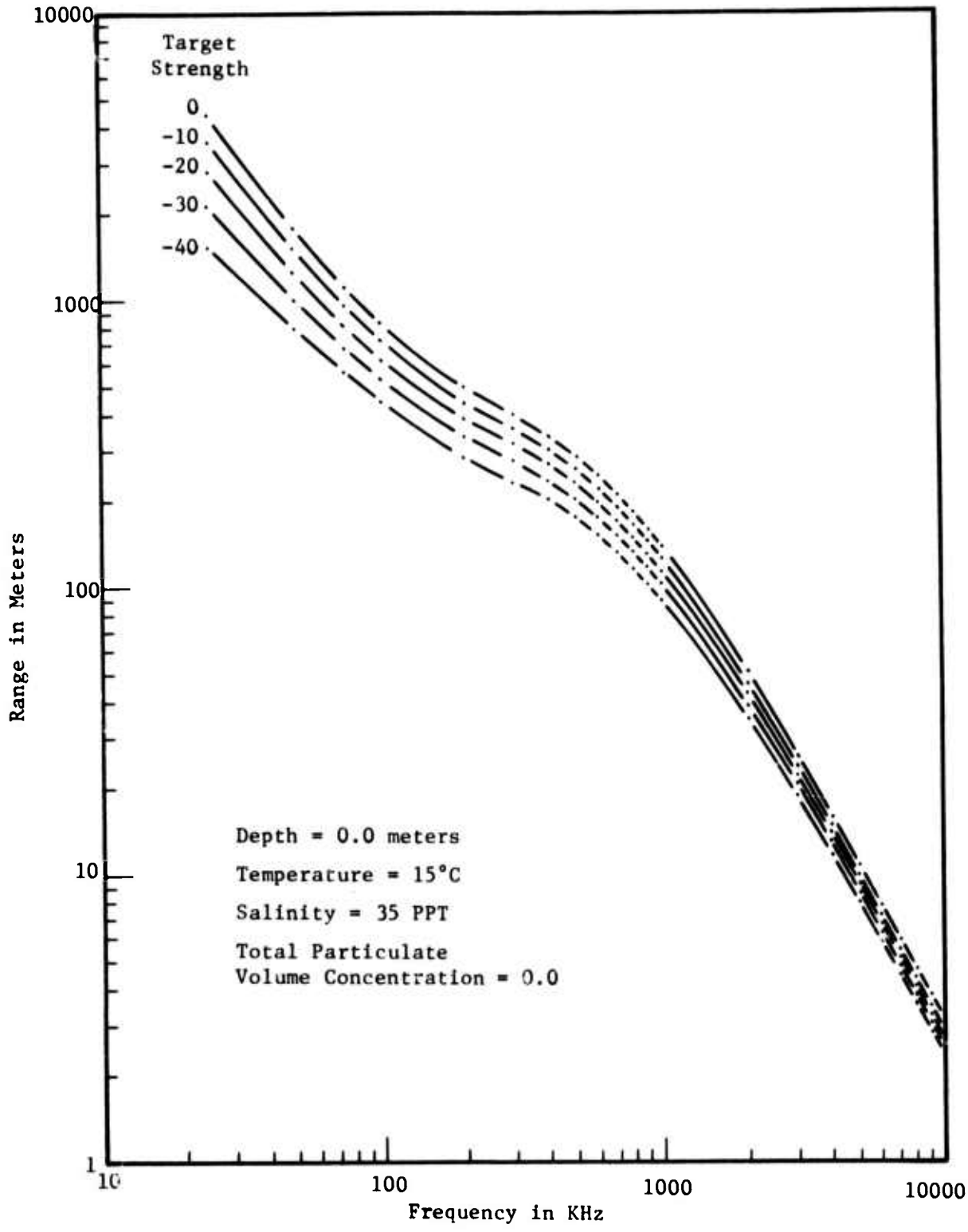

Figure 45: Dependence of range as a function of frequency with target strength as a parameter.

Capability of the TRW approach is determined, in part, by the characteristics of a photosensor array which is used to pick up diffracted light. The unit shown in Figure 46 will image in both cross-range directions if the photosensor array is a two-dimensional array. A good approach to generation of a visual image from the light diffracted onto the photosensor array uses a narrow-band amplifier following each photosensor in the image pickup array. This approach is economical because large scale integration techniques can be used to create several thousand amplifiers and photosensors in a sensor array with an overall dimension on the order of one inch on each side.

The narrow-band amplifier is important to obtain maximum sensitivity. The output of each narrow-band amplifier following each photosensor is integrated and stored for the intersample time. In this way, a signal is collected full time. The image is formed from the output of all narrow-band amplifiers collectively by multiplexing the respective outputs onto a single video wire. There is considerable flexibility in the output scan pattern; however, a good approach would be to duplicate the pattern used in the standard commercial television system. Here the outputs of amplifiers associated with photodiodes along a row are sequentially sampled row by row. This is accomplished by generating a scan signal which will close respective switches in the necessary pattern. Figure 46 illustrates this sytem. The standard clock for digital systems is used to synchronize a scan generator and a sweep generator which will move the image forming spot in synchronism to the photodiode which is sampled at any specific time. The circuit for generating the sweep would be particularly simple since it can be accomplished with little more than integration of a uni-polar pulse from the clock.

One application of the system would involve recording images in view as the supporting vessel moves along. In this way, the images are collected for subsequent viewing after a large field of view has been stored. The high resolution capability is possible together

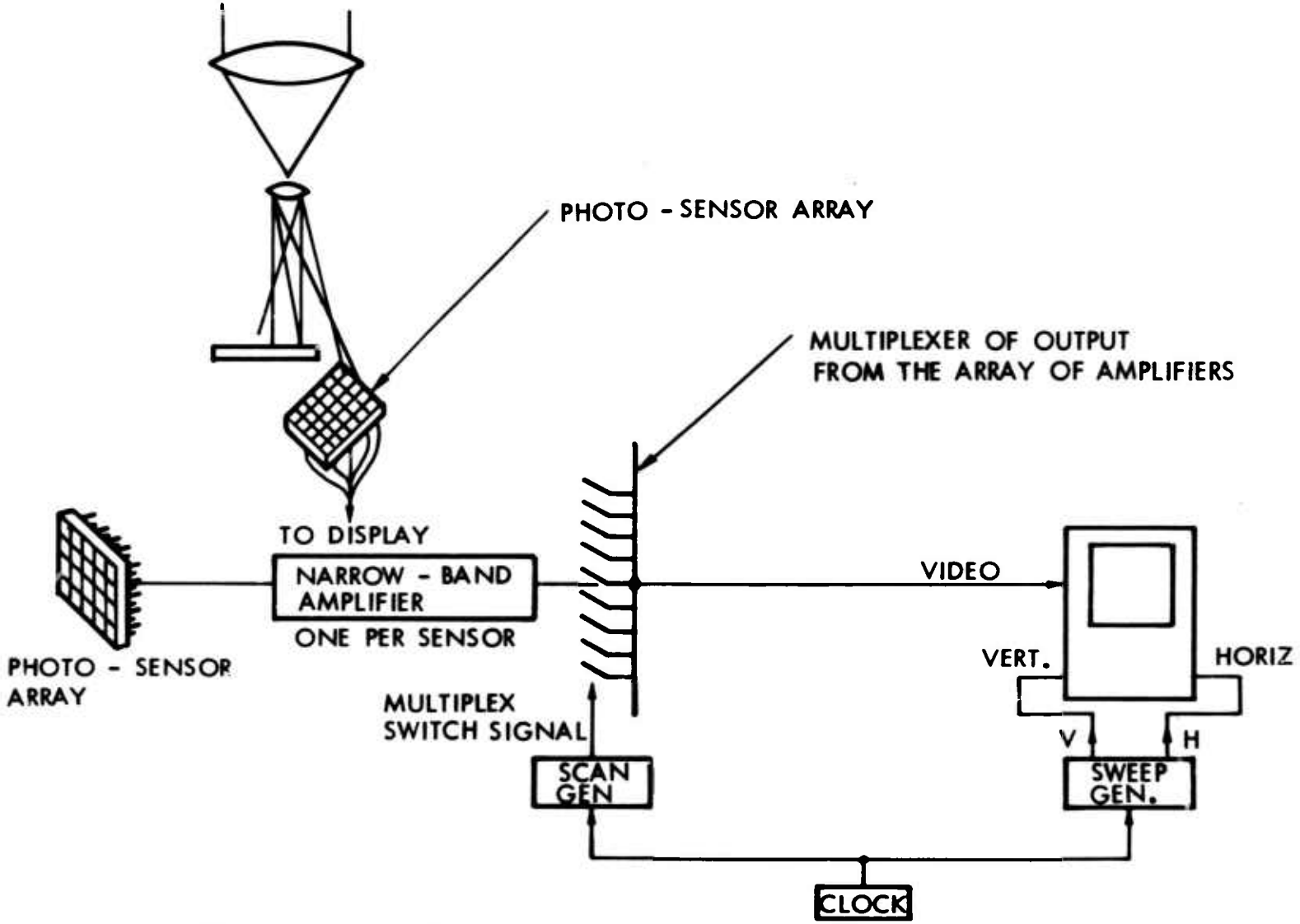

Figure 46: Signal processing in the TRW acousto-optical imaging sonar.

with a large field of view when this approach is used. A standard videotape recorder would be ideal for this application.

5.0 CONCLUSION

Laboratory experiments have demonstrated that the TRW acousto-optical approach to the construction of a high resolution imaging sonar is entirely feasible. Good images were formed from sound reflected by small objects located at the maximum distance possible in the existing laboratory facility. Cross-range resolution was checked and observed to lie within a factor of 3 of the maximum limit predicted by theory. This is about as good as expected without the use of high quality, nearly diffraction limited optics. Threshold sensitivity was measured and observed to be sufficiently good to obtain a range in excess of 300 meters in sea water. (Further improvements in sensitivity and projected range are expected because isolated system noise sources can be reduced by introduction of system improvements.)

A key advantage of the acousto-optical imaging sonar was shown to be its ability to provide two-dimensional imaging; that is, resolution in both the vertical and azimuthal planes. There are several applications in tactical situations where two-dimensional imaging can be of a distinct advantage. Reverberations limit the range capability of conventional sonars in many situations. Imaging separates signals arriving from different directions which eliminates the degrading effect of reverberations. In addition, a number of high resolution, short range applications require an imaging capability for close-up object identification and inspection. It is difficult to stretch conventional sonar to this capability because of the complexity of the approximately 10,000 beam channels which would be required[16]. On the other hand the acousto-optical imaging sonar can be extended to provide this capability because it directly employs optical LSI sensor arrays. Simplicity of electronic information processing results from direct conversion of acoustic phase front information to an optical image and display of the optical image from a photodetector array.

A significant feature of the TRW acousto-optical imaging approach (which uses double frequency heterodyning) is that the system discriminates incoming sound from outgoing sound (such as ship noise). (This feature is not possible with conventional hydrophones.) Experiments in our laboratory showed that the lab setup possessed a 35 db rejection of sound waves arriving from the unwanted direction of sensitivity.

Phase two of the project is presently underway. An improved laboratory acousto-optical imaging system is being assembled. Major emphasis during the second phase will be in achieving greater system sensitivity, improved cross range resolution and enhanced field of view.

TRW SYSTEMS GROUP

6.0 REFERENCES

1. A. Korpel, "Visualization of the Cross-Section of a Sound Beam for Bragg Diffraction of Light," Appl. Phys. Letters, 9:425-427 (15 Dec. 1966).

2. G. Wade, C. J. Landry and A. A. deSouza, "Acoustic Transparencies for Optical Imaging and Ultrasonic Diffraction," presented at the First International Symposium on Acoustical Holography, Huntington Beach, Calif., 1967 [Subsequently published in Acoustical Holography, edited by A. F. Metherell, H.M.A. El-Sum, and Lewis Larmore (Plenum Press, Inc., New York, 1969), Vol. I].

3. A. Korpel, "Acoustic Imaging by Diffracted Light. I. Two-dimensional Interaction," IEEE Trans. on Sonics and Ultrasonics, SU-15(3): 153-157 (July 1968).

4. J. Landry, J. Powers and G. Wade, "Ultrasonic Imaging of Internal Structure by Bragg Diffraction," Appl. Phys. Letters, 15(16):186-188 (15 September 1969).

5. R. Aprahamian, J. L. Jacoby and P. G. Bhuta, "Nondestructive Testing Using TRW Acousto-Optical Imaging System," Army Materials and Mechanics Research Center Report AMMRC CR 71-4/2, August 1971.

6. D. L. Folds, "Acoustic Imaging and High Resolution Sonar," (U) High Resolution Sonar Technology, Vol. II, March 1969. Confidential report prepared by the High Resolution Sonar Study Panel of the Mine Advisory Committee, NAS-NRC Washington, D.C.

7. D. T. Pierce and R. L. Byer, "Experiments on the Interaction of Light and Sound for the Advanced Laboratory," Amer. Jour. of Physics, Vol. 41:314-325 (March 1973).

8. C. V. Raman and N. S. Nagendra Nath, Proc. Indian Acad. Sci., Vol. 2, 413 (1935).

9. J. W. Goodman, Introduction to Fourier Optics, McGraw-Hill Book Co. (1963).

10. J. Landry, R. A. Smith and G. Wade, "Optical Heterodyne Detection in Bragg Imaging," Acoustical Holography, Vol. III, A. F. Metherell Ed., Plenum Press, 1971.

11. L. L. Higgins, et al., "Acoustic Bubble Detection," TRW Systems Report No. 12833-6006-RO-00 (31 March 1971).

12. R. A. Smith, et al, "Studies of Resolution in a Bragg Imaging System," J. Acoustical Soc. of Amer., V. 49, No. 3, (Part 3), pages 1062-1068, March 1971.

13. R. J. Urick, Principles of Underwater Sound for Engineers, McGraw-Hill Book Co., page 20, 1967.

14. E. G. McLeroy, "A Brief Analysis of the Effect of Solid Particles on Sonar Performance," U.S. Navy Mine Defense Lab., Panama City, Florida Report 1-100 (March 1966).

15. L. E. Kinsler and A. R. Frey, Fundamentals of Acoustics, John Wiley (1950).

16. "High Resolution Sonar Technology (U)," Vol. I - Summary, Conclusions, and Recommendations in Relation to Operational Navy Requirements (U), Control No. 69-R-1112, January 1969, Confidential; Vol. II, A Collection of Background Papers (U), Control No. 69-R-1367, March 1969, Confidential. Prepared by High Resolution Sonar Study Panel of the Mine Advisory Committee.

TRW SYSTEMS GROUP

APPENDIX A

CALCULATION OF ACOUSTIC FIELD INTENSITIES FOR DETERMINING SYSTEM SENSITIVITY

System sensitivities were calculated using an intensity distribution function (Ref. 15) applicable for circular piston transducers.

$$I_o = \frac{\rho c k^2 U_o S^2}{8\pi^2 R^2} \quad \text{and} \quad P_{av} = \frac{1}{2} \rho c S U_o^2$$

or

$$I_o = \frac{\pi a^2 f^2 P_{av}}{c^2 R^2}$$

where I_o = intensity of the circular piston main beam

P_{av} = average input power

ρ = density of water

c = sound speed in water

a = radius of the circular piston

$S = \pi a^2$ = surface area of the piston

U_o = velocity amplitude of the piston surface

f = acoustic frequency

$k = 2\pi f/c$ = acoustic wave number

R = range

The minimum detectable echo was calculated using the standard sonar equation for one way transmission (Ref. 13)

$$EL = SL - TL$$

where EL = minimum detectable echo

$SL = 71.5 + 10 \log P + DI_T$ = source level

P = power

$DI_T = 10 \log (\pi D/\Lambda)^2$

D = diameter of the circular piston

Λ = acoustic wavelength

$TL = 20 \log R + \alpha R \times 10^{-3}$

R = range

α = logarithmic absorption coefficient

The sensitivity results are listed in Tables A1 and A2 below for frequencies of 50, 160 and 500 KHz.

Table A1: System Sensitivity with Acoustic Lens.

Frequency	Intensity	Minimum Detectable Echo
500 KHz	9.3×10^{-12} watts/cm^2	11.4 db
160 KHz	1.9×10^{-12} watts/cm^2	5.3 db
50 KHz	1.9×10^{-13} watts/cm^2	-4.7 db

Table A2: System Sensitivity Without Acoustic Lens.

Frequency	Intensity	Minimum Detectable Echo
500 KHz	3.9×10^{-13} watts/cm^2	-2.3 db
160 KHz	9.6×10^{-14} watts/cm^2	-8.4 db
50 KHz	9.6×10^{-15} watts/cm^2	-18.4 db

These measurements were taken with the incident light intensity and modulation at an optimum level. This was previously determined and typical results are shown in Figure A1.

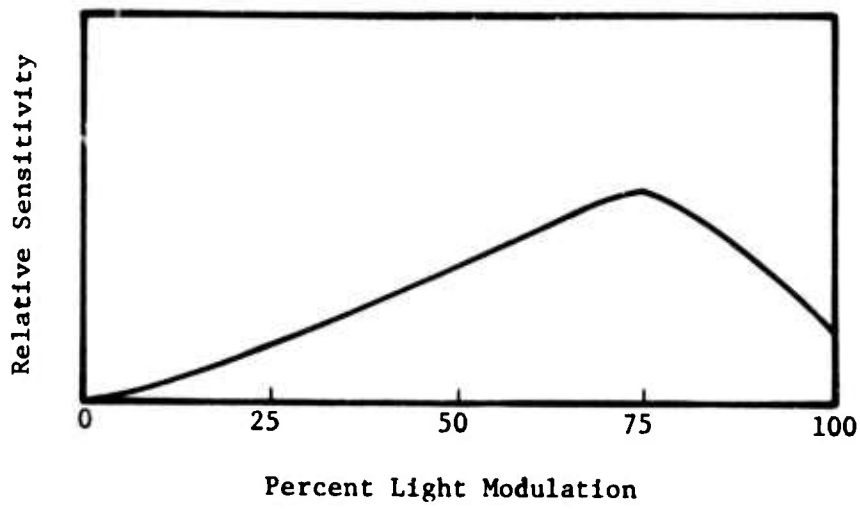

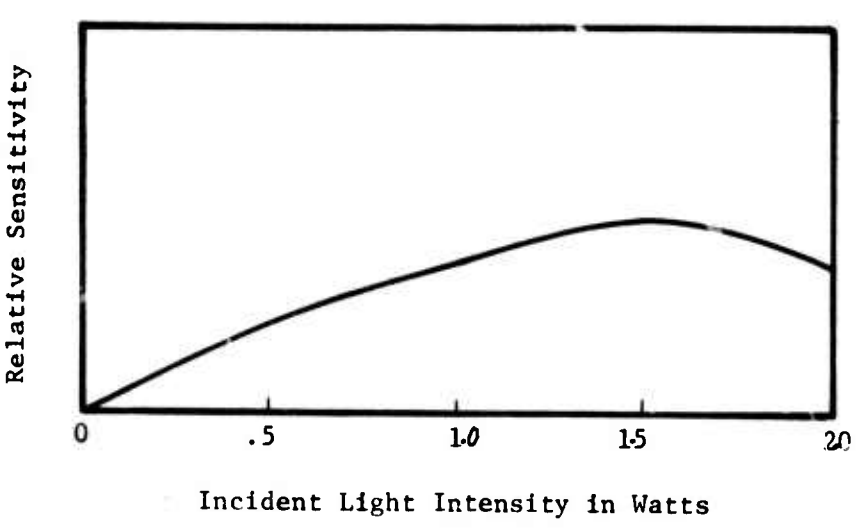

Figure A1: Sensitivity dependence at 500 KHz as a function of incident light intensity and modulation.

TRW
SYSTEMS GROUP

APPENDIX B

COMPUTER PROGRAM FOR PREDICTING IMAGING SONAR P .RFORMANCE

Projected performance of the TRW acousto-optical imaging sonar was calculated using the Fortran program listed in this appendix.

```
      PROGRAM OB (INPUT,OUTPUT,TAPE5=INPUT,TAPE6=OUTPUT)
      REAL KAPPA,MU(9,11)
      DIMENSION B(8),FT(9),V(9,11,9),ETA(9),RHO(9,11),
     1RHOO(9),KAPPA(9),D(11),P(9,11),T(9),S(9),F(10)
      DATA B/1.35E-2/,B/2.68E-2/
      DATA DO/1.0/,DIRECT/0.0/
      DATA A0/1.40295E3/,A1/5.04411497177/,A2/-5.52854935164E-2/,
     1A3/2.41590759023E-4/,A4/1.24994448604/,A5/2.29487467399E-3/,
     2A6/1.57267451618E-1/,A7/2.04834941313E-5/,A8/-1.33395409949E-2/,
     3A9/1.01470710283E-4/,A10/-8.35657086395E-7/,A11/2.89033197150E-7/,
     4A12/-2.00539914999E-10/,A13/4.18588753055E-5/
      DATA PI/3.141592/,RHOF/2.65E-3/
      DATA AA/4.E-6/
      DISPLAY (6) *T(1) IT TINC D(1) ID DINC S(1) IS SINC*
      ACCEPT T(1),IT,TINC,D(1),ID,DINC,S(1),IS,SINC
      DISPLAY (6) *F(1) IF FINC C(1) IC CINC*
      ACCEPT F(1),IF,FINC,C(1),IC,CINK
      DO 1 I=1,IT
      DISPLAY (6) *T=*,T(I),*RHOO      KAPPA*
      ACCEPT RHOO(I),KAPPA(I)
   96 RHOO(I)=RHOO(I)*1.E-3
      KAPPA(I)=KAPPA(I)/1.019716
      FT(I)=21.9*10.**(6.-1520./(T(I)+273.))
      IF (T(I).GT.20.) GO TO 101
      ETA(I)=1301./(998.333+8.1855*(T(I)-20.)+0.00585*(T(I)-20
     1.)**2)-3.30233
      ETA(I)=ETA(I)*2.30258509299
      ETA(I)=EXP(ETA(I))
      GO TO 500
  101 ETA(I)=((1.3272*(20.-T(I))-0.001053*(T(I)-20.)**2)/(T(I)+105.))
      ETA(I)=ETA(I)*2.30258509299
      ETA(I)=(EXP(ETA(I)))*0.01002
  500 CONTINUE
      DO 2 J=1,ID
      D(J)=D(J)*1.E+2
      P(I,J)=1.03323
      N=1
  104 A=RHOO(I)*D(J)*EXP(KAPPA(I)*(P(I,J)-1.03323))+1.03323-P(I,J)
      IF (ABS(A).LT.1.E-6)   GO TO 109
      APRIME=RHOO(I)*D(J)*KAPPA(I)*EXP(KAPPA(I)*(P(I,J)-1.03323))-1.
      P(I,J)=P(I,J)-A/APRIME
      IF (N.GT.100) GO TO 106
```

```
      N=N+1
      GO TO 104
  106 P(I,J)=1.0E+30
  109 D(J)=D(J)*1.E-2
      RHO(I,J)=RHOO(I)*1.E3*EXP(KAPPA(I)*(P(I,J)-1.03323))
      MU(I,J)=ETA(I)/RHO(I,J)
      SIGMA=RHOP/RHO(I,J)
      DO 3 K=1,IS
      V(I,J,K)=A0+A1*T(I)+A2*T(I)*T(I)+A3*T(I)**3+A4*S(K)+A5*S(K)*S(K)+
     1A6*P(I,J)+A7*P(I,J)*P(I,J)+A8*T(I)*S(K)+A9*T(I)*T(I)*S(K)+
     2A10*T(I)*P(I,J)*P(I,J)+A11*T(I)**3*P(I,J)+A12*S(K)*P(I,J)**3+
     3A13*T(I)*S(K)*P(I,J)
      DO 4 L=1,IF
      CONST=10.*ALOG10(2.38E-6*F(L)**2)-117.
      DIRECT=10.*ALOG10((PI*DD*F(L)*1.0E3/V(I,J,K))**2)
      IF (DIRECT.LT.0.0) DIRECT=0.0
      CONST=(CONST-DIRECT)/2.
      ALPHA=(Q*S(K)*FT(I)*F(L)*F(L)/(FT(I)*FT(I)+F(L)*F(L))+
     1B*F(L)*F(L)/FT(I))*(1.-6.54E-4*0.957841*P(I,J))*1.0936133
      BETA=SQRT(PI*F(L)*1.0E+03/MU(I,J))
      ABETA=BETA*AA*1.0E+02
      SI=(9./(4.*ABETA))*(1.+1./ABETA)
      TAU=0.5+9./(4.*ABETA)
      U=2*PI*F(L)*1.0E+03/V(I,J,K)
      CINC=CINK
      C(1)=0.0
   97 DO 5 M=1,IC
      ALFAP=U**4*AA**3/3.+(U*(SIGMA-1.)**2)*(SI/(SI**2+(SIGMA+TAU)**2))
      R1=5.0E3
      R2=1.0E-30
      R=(R1+R2)/2.0
      NN=1
    7 W=20.*ALOG10(R)+ALPHA*R*1.E-3+C(M)*ALFAP*R+CONST
      IF (ABS(W).LT.1.E-3) GO TO 6
      IF (W) 50,5,51
   50 R2=R
      R=(R1+R)/2.0
      GO TO 55
   51 R1=R
      R=(R+R2)/2.0
   55 CONTINUE
      IF (NN.GT.100) GO TO 5
```

```
      IF (R.LE.0.0)  GO TO 6
      NN=NN+1
      GO TO 7
    6 ALFAP=ALFAP*C(M)
      DISPLAY (6) *RANGE                    COND        ALFAP*
      DISPLAY (6) R,C(M),ALFAP
      IF (IC.EQ.1) GO TO 5
      QQ=(-1.0)**4
      IF (QQ) 9,8,8
    9 C(M+1)=.001*CINC
      GO TO 5
    8 C(M+1)=.005*CINC
      CINC=CINC*10.
    5 CONTINUE
      DISPLAY (6) *FREQ        ALPHA*
      DISPLAY (6) F(L),ALPHA
      F(L+1)=F(L)+FINC
    4 CONTINUE
      DISPLAY (6) *SALT         VELOCITY*
      DISPLAY (6) S(K),V(I,J,K)
      S(K+1)=S(K)+SINC
    3 CONTINUE
      DISPLAY (6) *DEPTH         PRESSURE                    RHO*
      DISPLAY (6) D(J),P(I,J),RHO(I,J)
      D(J+1)=D(J)+DINC
    2 CONTINUE
      DISPLAY (6) *TEMP            RHOO        ETA           KAPPA*
      DISPLAY (6) T(I),RHOO(I),ETA(I),KAPPA(I)
      T(I+1)=T(I)+TINC
    1 CONTINUE
      STOP
      END
```